ACOUSTOOPTIC SPECTRUM ANALYSIS AND NARROWBAND INTERFERENCE EXCISION IN WIDEBAND SIGNAL ENVIRONMENTS

F. Weldon Regan

NPS62-79-011

NAVAL POSTGRADUATE SCHOOL
Monterey, California

THESIS

Acoustooptic Spectrum Analysis
And Narrowband Interference Excision
In Wideband Signal Environments

F. Weldon Regan, III

September 1979

Thesis Advisor: J. P. Powers

Prepared for:
Naval Elctronic Systems Command (ELEX350)
Washington, D.C. 20360

SECURITY CLASSIFICATION OF THIS PAGE (When Data Entered)

REPORT DOCUMENTATION PAGE

READ INSTRUCTIONS BEFORE COMPLETING FORM

1. REPORT NUMBER: NPS-62-79-011	2. GOVT ACCESSION NO.
3. RECIPIENT'S CATALOG NUMBER	
4. TITLE (and Subtitle): Acoustooptic Spectrum Analysis and Narrowband Interference Excision in Wideband Signal Environments	5. TYPE OF REPORT & PERIOD COVERED: Thesis Report; 1Oct75-30Sept79
	6. PERFORMING ORG. REPORT NUMBER
7. AUTHOR(s): F. Weldon Regan, III	8. CONTRACT OR GRANT NUMBER(s)
9. PERFORMING ORGANIZATION NAME AND ADDRESS: Naval Postgraduate School, Monterey, California 93940	10. PROGRAM ELEMENT, PROJECT, TASK AREA & WORK UNIT NUMBERS
11. CONTROLLING OFFICE NAME AND ADDRESS: Naval Electronic Systems Command(ELEX-350), Washington, D.C. 20360	12. REPORT DATE: September 1979
	13. NUMBER OF PAGES: 113
14. MONITORING AGENCY NAME & ADDRESS(if different from Controlling Office)	15. SECURITY CLASS. (of this report): Unclassified
	15a. DECLASSIFICATION/DOWNGRADING SCHEDULE

16. DISTRIBUTION STATEMENT (of this Report)
Approved for public release; distribution unlimited.

17. DISTRIBUTION STATEMENT (of the abstract entered in Block 20, if different from Report)

18. SUPPLEMENTARY NOTES

19. KEY WORDS (Continue on reverse side if necessary and identify by block number)
Bragg cell
Acoustooptics
Spectrum Analyzer
Optical Excision

20. ABSTRACT (Continue on reverse side if necessary and identify by block number)
This thesis is a study of performance measures for acoustooptic spectrum analysis, and optical excision of narrowband interference. A Gaussian laser beam model is developed and programmed for propagation through thin lenses. Effects of beam truncation by Bragg cell apertures are examined. Bragg cell performance is analyzed with respect to diffraction efficience, information capacity, and response agility. A performance comparison is made between charge-coupled device and photodiode technologies in photodetector array

DD FORM 1 JAN 73 1473 EDITION OF 1 NOV 65 IS OBSOLETE
S/N 0102-014-6601 |
(Page 1)

SECURITY CLASSIFICATION OF THIS PAGE (When Data Entered)

applications. Overall excisor performance is discussed in terms of interference removal effectiveness and process corruption of residual information bearing signals.

Approved for public release; distribution unlimited

Acoustooptic Spectrum Analysis And Narrowband Interference Excision In Wideband Signal Environments

by

F. Weldon Regan, III
Lieutenant, United States Navy
B.S.E.E., University of Michigan, 1973

Submitted in partial fulfillment of the requirements for the degree of

ELECTRICAL ENGINEER

from the

NAVAL POSTGRADUATE SCHOOL
September 1979

ABSTRACT

This thesis is a study of performance measures for acoustooptic spectrum analysis, and optical excision of narrowband interference. A Gaussian laser beam model is developed and programmed for propagation through thin lenses. Effects of beam truncation by Bragg cell apertures are examined. Bragg cell performance is analyzed with respect to diffraction efficiency, information capacity, and response agility. A performance comparison is made between charge-coupled device and photodiode technologies in photodetector array applications. Overall excisor performance is discussed in terms of interference removal effectiveness and process corruption of residual information bearing signals.

TABLE OF CONTENTS

I. INTRODUCTION- 9

A. OVERVIEW- 9

B. THESIS OBJECTIVE- - - - - - - - - - - - - - - - 10

C. A-O SPECTRUM ANALYSIS - - - - - - - - - - - - - 11

D. OPTICAL EXCISION- - - - - - - - - - - - - - - - 14

E. SPECIFIC GOALS- - - - - - - - - - - - - - - - - 17

F. PERSPECTIVE - - - - - - - - - - - - - - - - - - 21

II. PERFORMANCE GUIDELINE ANALYSIS- - - - - - - - - - 23

A. PARAMETERS OF NEGLIGIBLE EFFECT - - - - - - - - 23

B. LASER BEAM PROPAGATION- - - - - - - - - - - - - 25

C. BRAGG CELL PERFORMANCE- - - - - - - - - - - - - 48

D. PHOTODETECTOR PERFORMANCE - - - - - - - - - - - 78

E. OPTICAL AND ELECTRONIC CLIPPING MODELS- - - - 84

III. SUMMARY/RECOMMENDATIONS - - - - - - - - - - - - - 96

A. RESULT SUMMARY- - - - - - - - - - - - - - - - - 96

B. RECOMMENDATIONS - - - - - - - - - - - - - - - - 97

C. AREAS FOR FURTHER ANALYSIS- - - - - - - - - - - 97

D. CONCLUSION- - - - - - - - - - - - - - - - - - - 98

APPENDIX A - BEAM RADIUS AND SPOT SIZE PLOT PROGRAM - - 99

APPENDIX B - GAUSSIAN PROPAGATION PROGRAM - - - - - - -101

APPENDIX C - BANDSHAPE PROGRAM- - - - - - - - - - - - -104

APPENDIX D - NARROW OBSTACLE DIFFRACTION PROGRAM- - - -106

LIST OF REFERENCES- - - - - - - - - - - - - - - - - - -109

INITIAL DISTRIBUTION LIST - - - - - - - - - - - - - - -112

LIST OF FIGURES

1. Optical Clipping Process Sequence- - - - - - - - - - 15

2. Gaussian Beam Characteristics- - - - - - - - - - - - 27

3. Phase Front Radius as a Function of Propagation Distance - 28

4. Beam Spot Size as a Function of Distance - - - - - - 29

5. Gaussian Beam Transiting Thin Lens - - - - - - - - - 31

6. Experimental Acoustooptic Spectrum Analyzer- - - - 34

7. Photodetector Array Output - - - - - - - - - - - - - 39

8. Photo Element Dimensional Diagram- - - - - - - - - - 40

9. Maximum Sidelobe Level vs Truncation Ratio - - - - 44

10. Graded Transmission Profile- - - - - - - - - - - - - 47

11. Bragg cell Operation - - - - - - - - - - - - - - - - 49

12. Diffraction Efficiency Bandshape - - - - - - - - - - 53

13. First Order Stepped Array- - - - - - - - - - - - - - 60

14. NPS A-O Spectrum Analyzer Display of Wideband FM Signal- 79

15. Conventional Spectrum Analyzer Display of Same Wideband FM Signal as in Figure 14 - - - - - - - - 79

16. CCD Photodetector Array Chip Schematic - - - - - - 81

17. CCPD Photodetector Array Chip Schematic- - - - - - 82

18. Narrow Obstacle in Plane-Wave Light Field- - - - - 86

19. Narrow Obstacle Diffraction Model Schematic- - - - 87

20. Diffracted Light Intensity Profile for: r_o = 102 um; Δy=16 um- - - - - - - - - - - - - - - - 88

21. Diffracted Light Intensity Profile for: r_o = 160 um; Δy=16 um- - - - - - - - - - - - - - - - 89

22. Diffracted Light Intensity Profile for: r_o = 284 um; Δy=16 um- - - - - - - - - - - - - - - - 90

23. Diffracted Light Intensity Profile for: r_o = 640 um; Δy=16 um- - - - - - - - - - - - - - - - 91

24. Diffracted Light Intensity Profile for:
r_o = 2.5 um; Δy-16 um- - - - - - - - - - - - - - - - 92

25. Diffracted Light Intensity Profile for:
r_o = 10 mm; Δy=16 um - - - - - - - - - - - - - - - - 93

26. Diffracted Light Intensity Profile for:
r_o = 1.2 m; Δy=16 mm - - - - - - - - - - - - - - - - 94

LIST OF TABLES

I. PROPAGATION PROGRAM INPUTS- - - - - - - - - - - - - 35

II. PROPAGATION PROGRAM INTERMEDIATE RESULTS- - - - - 42

III. COMPARISON OF BEAMWIDTH VALUES- - - - - - - - - - 43

I. INTRODUCTION

A. PROBLEM OVERVIEW

The increased use of spread spectrum communication and ranging techniques has necessitated rethinking of interception scheme implementations. Two common requirements of many receiver systems operating in this wideband environment are: adequate spectrum analysis, and effective excision of narrowband high power interference. Acoustooptic spectrum analysis and optical interference excision are two demonstrable methods of fulfilling these respective requirements.

An acoustooptic spectrum analyzer transforms a wideband time domain signal into a spatially detected frequency domain signal. An optical excisor at the detector can also utilize this space-time transformation. It performs real-time notch filtering of narrowband interference. Specific operational applications of the two devices include broadband receiver, radar and surveillance systems. All three military services rely on these systems and need good interference rejection. To meet this need, a NAVELEX 350/DARPA program was funded for the development of optical excision techniques.

The technical objectives of this effort are to:

1. Survey potential applications and analyze technical requirements imposed by each.
2. Analyze alternative optical excision configurations and components.

3. Develop/procure major system components.

4. Fabricate and measure alternative broadband excisor configurations to verify analytical results.

5. Fabricate and field test a brassboard model.

6. Design a preliminary advanced development model.

The principal civilian contractor for the project is PROBE Systems, Inc. PROBE, assisted by the development efforts at the Naval Research Laboratory (NRL) and Naval Postgraduate School (NPS), was tasked with attainment of these objectives. NRL's specific program assistance was the development of a photodichroic optical clipper to be evaluated by PROBE. The research summarized in this thesis is part of the NPS contribution to the development program.

B. THESIS OBJECTIVE

The objective of this work effort was to conduct a performance analysis of acoustooptic (a-o) spectrum analyzer and optical excisor components. The choice of this goal, over other possible goals related to the development program, allows maximal use of the Postgraduate School's substantial technical library and computer facilities. The approach was also felt to be the best way to augment PROBE's experimental study and minimize duplicate effort. This resulting study is intended to benefit the program by providing a comprehensive set of "first cut" performance guidelines.

This objective was divided into four specific aims. Each effort relates to a particular system component. A summary of these goals is provided in Section E. However, more

complete explanations of a-o spectrum analysis and optical excision are required beforehand.

C. ACOUSTOOPTIC SPECTRUM ANALYSIS

An acoustooptic spectrum analyzer is primarily composed of an a-o beam deflector, photodetector array, and a laser. Its operating sequence begins with an input rf signal which excites a piezoelectric transducer mounted on the acoustic medium of the a-o deflector or Bragg cell. The transducer launches an acoustic wavetrain through the medium. The wavetrain spatially modulates the refractive index and acts as a moving diffraction grating for the laser light. The acoustooptic interaction produces a one-dimensional angular pattern of diffracted beams. This pattern matches the spectral content of the original rf signal. Each individual beam intensity is directly proportional to the corresponding rf signal frequency component intensity. Beam deflection angles are directly proportional to the component frequencies. A thin convex lens is used to focus the diffraction pattern on an image plane linear detector array. Lastly, the array photosites video-detect the beam pattern and transfer the spectral information out electronically via shift registers.

This method of wideband spectrum analysis offers many features which are difficult to achieve by other means. For example, a conventional scanning spectrum analyzer suffers from several shortcomings when used as a wideband surveillance receiver. Signals, which utilize direct sequence and frequency hopping spread spectrum modulation techniques, prove difficult

to adequately monitor. Pulsed signals are also troublesome because their probability of intercept is low. An a-o spectrum analyzer readily accomplishes these surveillance tasks. Since the instantaneous bandwidth is very wide, probability of intercept problems are greatly diminished. The demonstrated output frequency resolution is excellent. These two features permit highly effective operation in densely populated signal environments. Also, the simpler physical components make the resulting equipment package smaller and less expensive than comparable conventional systems, especially in the case of integrated optic system versions.

Several articles which discuss currently available commercial units are listed in the bibliography. Reference 1 describes an ITEK a-o spectrum analyzer with a 500 MHz bandwidth and 1 MHz frequency resolution. Typical applications for this processor include broadband analysis and cueing receivers.

Reference 2 discusses GTE Sylvania's work to develop acoustooptic wideband receiver and direction finder systems, presenting an angle of arrival detection scheme which utilizes multichannel Bragg cells. A GTE receiver having a 1 GHz bandwidth and frequency resolution of 2.6 MHz is also mentioned.

A snapshot overview of acoustooptic development programs is related in Ref. 3. The article discusses recent advances made by the above two companies and related work done by others. It also examines exploratory work in integrated optic circuit chips. Hughes, Rockwell International, and Westinghouse are the major companies deeply involved in this.

In addition to the above articles, the bibliography also notes a few landmark research papers. Reference 4 is the first article in this category. It is an excellent review of acoustooptic historical aspects which covers progress beginning with Brillouin's 1922 prediction of light scattering by thermally generated acoustic waves. In this work, C. G. Quate and his associates neatly condensed much of the primarily academic work done prior to the 1960's. They also conducted a thorough two-dimensional analysis of wave interactions.

The invention of the laser in the early sixties significantly increased the practical application possibilities of acoustooptic devices. Some of the first attempts to utilize the Bragg cell are discussed in Ref. 5. The authors, A. Korpel and others, explored the feasibility of acoustooptic television displays. They presented, in addition to the experimental findings, an analysis of one of the first a-o beam deflectors having a stepped transducer. The special transducer steered the acoustic wavetrain to maximize the proper light-sound interaction. This "beam steering" technique increased the effective operating bandwidth of the Bragg Cell.

R. Adler, one of the pioneers who worked with Korpel, gave a clear summary of beam deflector principles in Ref. 6. He also discussed a wide variety of acoustooptic applications which included television displays, spectrum analyzers, and acoustic imagers.

Other references, which relate to specific analyzer aspects, are cited in following sections. However, the above

three papers best provide the flavor of development work and concisely present the significant acoustooptic principles.

D. OPTICAL EXCISION

The optical excision process utilizes all a-o spectrum analyzer components with the addition of an optical or electronic clipper. Only minor modifications are made in the operating sequence. The image plane diffraction pattern is generated in the same manner as previously discussed. The clipping action takes place in, or in front of, the image plane. Phase integrity is important for the time domain reconstruction of the signal, thus heterodyne-detection replaces video-detection to preserve signal phase.

If an electronic clipper is used, then the array photosite outputs must be individually serviced. Outputs which correspond to frequencies in the notch band are ignored. The remaining outputs are summed to produce an excised version of the input signal.

An optical clipper requires a single large area photodetector to recover the heterodyned signal. An opaque obstruction blocks or clips the diffracted beams produced by frequencies in the notch band. The remaining beams are mixed with a reference local oscillator beam and recovered by the detector. The net output is again an excised version of the input signal. A diagram of the optical clipping process is shown in Figure 1.

Optical excision has several advantages lacking in conventional approaches to narrowband interference rejection.

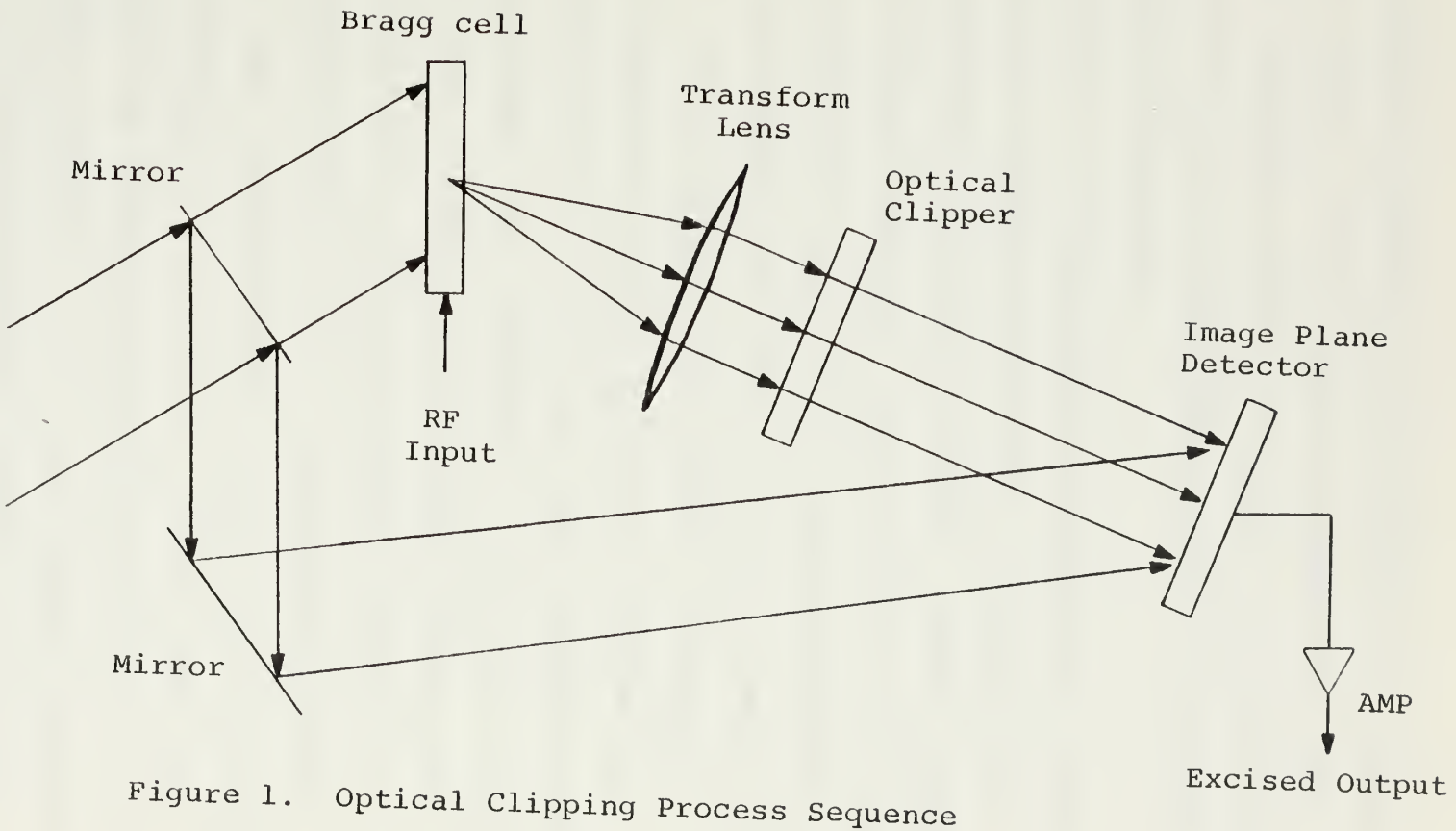

Figure 1. Optical Clipping Process Sequence

The process offers an arbitrary notch bandwidth with nearly infinite skirt slope. Optical excision lends itself well to adaptive notch filtering, which is important in signal environments having time-varying interference sources of arbitrary number and center frequencies.

Several efforts to develop suitable clippers are underway. Photodichroic crystals are one set of possible contenders for application in optical clippers. These crystals, when used with crossed polarizers, act as optical attenuators. The amount of attenuation is dependent upon the incident light intensity. This property gives them an inherent spatial filter capability. Strong interference signals are sharply attenuated or clipped, and weaker signals of interest pass through. As mentioned in the overview, NRL is deeply involved in this development area. Reference 7 provides a summary of experimental work on photodichroic spatial filters performed by W. C. Collins at the Naval Research Laboratory.

PROM's or Pockels Readout Optical Modulators also show promise in this area. A PROM optical clipper uses two lasers of different wavelengths. The first or "write" laser has a shorter wavelength and creates photoconductive spots on the PROM. These areas correspond to the interference frequencies to be excised. The PROM, positioned between crossed polarizers, is "read" by a laser of longer wavelength. Diffracted beams produced by the interference signal are blocked by the combined action of the photoconductive regions and crossed polarizers. The remaining diffracted beams are transmitted through the PROM and recovered by the heterodyned detector.

Reference 8 describes a PROM developed by ITEK which was used as part of an acoustooptic spectrum analyzer.

The LCLV or Liquid Crystal Light Valve is another possible optical clipper. Hughes Research Laboratory has been the principal developer. The device consists of a liquid crystal photoconductor sandwich which uses scattering centers to disrupt the coherence of incident laser light. The scattering centers are created by the interaction of a cross-sandwich electric field and the incident light intensity pattern. The incident light lowers the resistivity of the photoconductor sandwich portion in proportion to the intensity. This action increases the electric field in the liquid crystal layer and causes molecular alignment rotations. The areas of molecular rotation are the scattering centers. In order to be used as an optical clipper, the light valve is positioned between crossed polarizers. Attenuation is dependent upon molecular rotation and thereby the incident light intensity. Reference 9 discusses progress made by Hughes on the LCLV. The article also compares various spatial filters' performance including the three mentioned here.

E. SPECIFIC GOALS

The specific goals of this work were narrowed down to four principal areas. First, laser beam profile effects on signal frequency component resolution required study. Second, Bragg cell performance factors needed determination for optimal system design. Third, photodetector capabilities and effects required scrutiny to compare the advantages of competing

detector technologies. And fourth, optical excision needed modeling to determine process effectiveness. The following paragraphs expand on these points.

Laser light beam propagation was the first major aspect studied. This subject is important because the beam's cross-sectional behavior is a function of the propagation circumstances. The beam profile significantly affects both a-o spectrum analyzer and optical excisor performance.

For example, a wide beam is desired at the deflector aperture. This condition maximizes the acoustooptic interaction. Conversely, a small light beam cross section is necessary at the image plane to discriminate the input signal's frequency components.

Ray optics can not be used to determine beam profile behavior through the various system elements, as it does not adequately describe beam propagation characteristics. Fortunately, the complex variable equations, which do govern beam transmission through space and thin lenses, are available; however, they are cumbersome to use. Simple methods of dealing with them were needed to increase their usefulness as performance gauges. In particular, a hand-held calculator program was desirable to determine optimal lens placement and beam propagation indices.

Also, propagation through the Bragg cell's finite dimension aperture affects cross-sectional behavior. The abrupt windowing action truncates the beam profile and causes sidelobes to appear. These sidelobes, if sufficiently large, contribute erroneous frequency components to the image

plane. Investigation of this phenomenon was required to determine the degree of performance degradation.

The second thesis goal was to analyze factors affecting Bragg Cell performance. To pursue this goal, it was necessary to define good deflector performance. Uchida [10] did this concisely in terms of three criteria: high diffraction efficiency, large information capacity, and quick response.

Diffraction efficiency is the ratio of a diffracted light beam's intensity to that of the incident light beam. The input acoustic power is one of the components which determine diffraction efficiency. A higher input acoustic power will give a greater diffraction efficiency, but only at a price. Increased acoustic power heats the interaction medium and creates troublesome temperature gradients. Resolution suffers and information capacity is lowered. Damping of internal reflections is made more difficult, causing an undesirable persistence of signals which are no longer present. Deflectors which exhibit high diffraction efficiency with low acoustic power are very advantageous.

Information capacity can be measured simply as the number of resolvable diffracted beams. It can also be influenced by geometric factors. Stretching the interaction medium's acoustic path length will increase the number of resolvable frequencies. However, this approach will also slow responsiveness to changing signal environments.

Simultaneous achievement of all three criteria, high diffraction efficiency, large information capacity, and quick

response is not possible yet, but performance may be adequately tailored to a particular application by decreasing one unnecessary feature in order to increase a crucial one.

Photodetector performance was another important subject for analysis. Detector performance criteria include: dynamic range, resolution, and information bandwidth. For spectrum analysis applications, there are two contending device types. Either a Charge-Coupled Device (CCD) detector array or a Charge-Coupled PhotoDiode (CCPD) detector array may be used. Both arrays are composed of a linear grouping of photosites. The photosites detect and integrate incident light intensities. Their response sensitivity is matched to the laser wavelength. Dynamic range is limited by photosite saturation illumination and dark current. Resolution is limited by the number and linear packing density of the photosites. Information bandwidth is limited by electronic sampling considerations.

For optical excision applications which utilize an optical clipper, a single large area detector is required. Potential device types include photodiodes and photomultiplier tubes. A photodiode may be adequate for a particular system if the information bandwidth of the signal is not large. Photomultiplier tubes are available for wideband requirements. Dynamic range limitations are similar to those for detector arrays. Resolution is determined by the optical clipper and the diffracted beam spot size.

A number of references are available which highlight important aspects of the different detectors. CCD principles of operation are presented in Ref. 11. Reference 12 analyzes

photodiode array noise considerations in depth. Reference 13 includes mathematical examinations of video and heterodyne-detection for photodiodes and photomultiplier tubes.

Electronic and optical clipping methods comprised the final areas of analysis. Models of both techniques were developed. The first model addressed optical clipping.

The blocking action of an optical clipper may be modeled to a first order approximation as a narrow obstacle in a coherent plane wave light field. The corresponding image plane diffraction pattern can be described in terms of Fresnel integrals. These integrals may be approximated by numerical methods. The resulting computer plots help one to visualize diffraction effects produced by an optical clipper.

The next model is primarily associated with electronic clipping. It is intended to provide a measure of signal degradation which is induced by the excision process. This degradation which is caused by the removal of the desired signal's frequency components in the excisor's notch band. For Direct Sequence Spread Spectrum (DSSS) signals, this results in attenuation of the correlation peak. By comparison, degradation effects for frequency hopped signals are not considered here as these signals do not derive any benefits from the excision process.

F. PERSPECTIVE

The fundamental purpose of this introduction was to explain the motivations for the work effort. Primary justification for the undertaking was the same as for the sponsoring

development program--a real obstacle to effective utilization of spread spectrum techniques must be confronted. The problem of narrowband interference cannot reasonably be expected to diminish with only passage of time, more probably it will increase.

Acoustooptics promises a solution to this interference problem. The necessary technologies are maturing, and several available products ably handle missions similar to the intended ones discussed here. Therefore, this promised solution is very likely to be fulfilled in the near future.

II. PERFORMANCE GUIDELINE ANALYSIS

A. PARAMETERS OF NEGLIGIBLE EFFECT

Several secondary effects are present in both the a-o spectrum analyzer and optical excisor which were not considered as being germane to the thesis. Consequently, they were not examined in great detail. This section is a brief compilation of those effects.

One performance affecting parameter outside the analysis realm of this thesis is input noise contributed by the receiver system. No operation in either spectrum analysis or optical excision processors decreases white Gaussian noise. Above 50 MHz, atmospheric noise diminishes, and receiver noise figure becomes an important consideration. The intended applications for both systems are assumed to be above 50 MHz. However, the techniques dealing with receiver noise figure are well documented elsewhere and therefore are not addressed in this report. In all further analysis, the system noise induced prior to Bragg cell injection is assumed negligible.

External vibration is another potential problem in both a-o spectrum analyzers and optical excisors. Component mounting vibrations can introduce undesirable signal modulations. Air currents may also disturb the signal. Coherent detection schemes are particularly sensitive to both occurrences. Susceptibility to small ambient air currents was documented by M. King and his associates in Ref. 14. They

observed random phase modulation of a coherently detected signal which was caused by minor air movement. The experimental work of this thesis was done under controlled conditions with minimal mechanical disturbance. Also, video-detection, which reduced vibration concerns, was employed. In general, vibration considerations cannot be effectively encompassed within the framework of this report. The subject must be addressed with respect to each particular application.

Laser frequency stabilization requirements of the optical excisor coherent detection scheme were also briefly investigated. Stabilization was concluded to be unnecessary for this application as the reference local oscillator is derived from the same laser beam as the information signal. Frequency variations in the local oscillator are matched by those in the signal beam. Only if there were a large path length difference between the signal beam and local oscillator would there be any chance of beat frequencies appearing in the information band. This condition does not exist in the optical excisors previously described.

Tyndall scattering is a consideration in systems which employ liquid medium Bragg cells. It is not a concern with high purity crystal medium Bragg cells. Tyndall scattering is due to foreign suspended matter in the interaction medium. Scattering of this type contributes to background noise. It can be controlled by careful filtering of the liquid medium.

Liquid medium Bragg cells are restricted to operation under 100 MHz due to attenuation considerations. Most new Bragg cells employ low acoustic velocity crystals. The a-o

deflector, used in experiments related to this thesis, housed a crystalline interaction medium, therefore, discussion of this topic is limited here. For those interested, further remarks on Tyndall scattering are made in Ref. 15.

Temperature gradients in the Bragg cell medium have already been described in the introduction as harmful to information capacity. Reference 10 documents experimental observations of thermal gradient effects. This condition can be controlled in essentially three ways. First, keeping the input acoustic power low minimizes input heat. Second, employing materials with high thermal conductivity helps to maintain uniform heat content throughout the medium. Third, using external cooling aids in dissipating heat introduced by the transducer.

Nonuniformity of photosite responsivity for photodetector arrays is the last topic considered in this section. Typical variation for both CCD and CCPD arrays is ten percent above or below the mean. Normally, the intended applications do not require more exacting tolerances. In the event that such precision is required, digital compensation techniques may be employed to offset individual photosite deviations. Reference 12 contains more discussion on this subject.

B. LASER BEAM PROPAGATION

The first goal of the propagation study was to develop simple methods of dealing with the equations which govern transmission through space and thin lenses, and enable determination of beam spot size and phase front radius anywhere

within the optic train path. In order to explain the results of the effort more concisely, a brief review of laser propagation fundamentals is presented. This review is based on a treatment provided in Ref. 16.

The type of laser beam source discussed throughout this paper is a standard Helium-Neon unit which radiates at a .6328 micron wavelength. The beam has a Gaussian intensity profile and a spherical phase front. Beam spot size is defined as the perpendicular distance from the beam centerline to a point where the intensity has dropped by $1/e^2$ factor. Beam radius is the phase front curvature radius. These two quantities uniquely determine the characteristics of free space Gaussian beam propagation. The plane perpendicular to the propagation path, where the spot size is a minimum and the radius is infinite, is referred to as the "waist" and is shown in Figure 2.

Two equations determine beam spot size and radius as a function of directed propagation distance. Plots of beam radius and spot size, for propagation through free space, are depicted in Figs. 3 and 4. The equations are:

$$\text{Beam Radius} = R(z) = z + \{\pi w_o^2/\lambda\}^2/z \qquad (1)$$

$$\text{Beam Spot Size} = w(z) = w_o\{1 + \{\lambda z/\{\pi w_o^2\}\}^2\}^{1/2} \qquad (2)$$

where:

w_o = Minimum Beam Spot Size

λ = Laser Wavelength

z = Propagation Distance from Waist

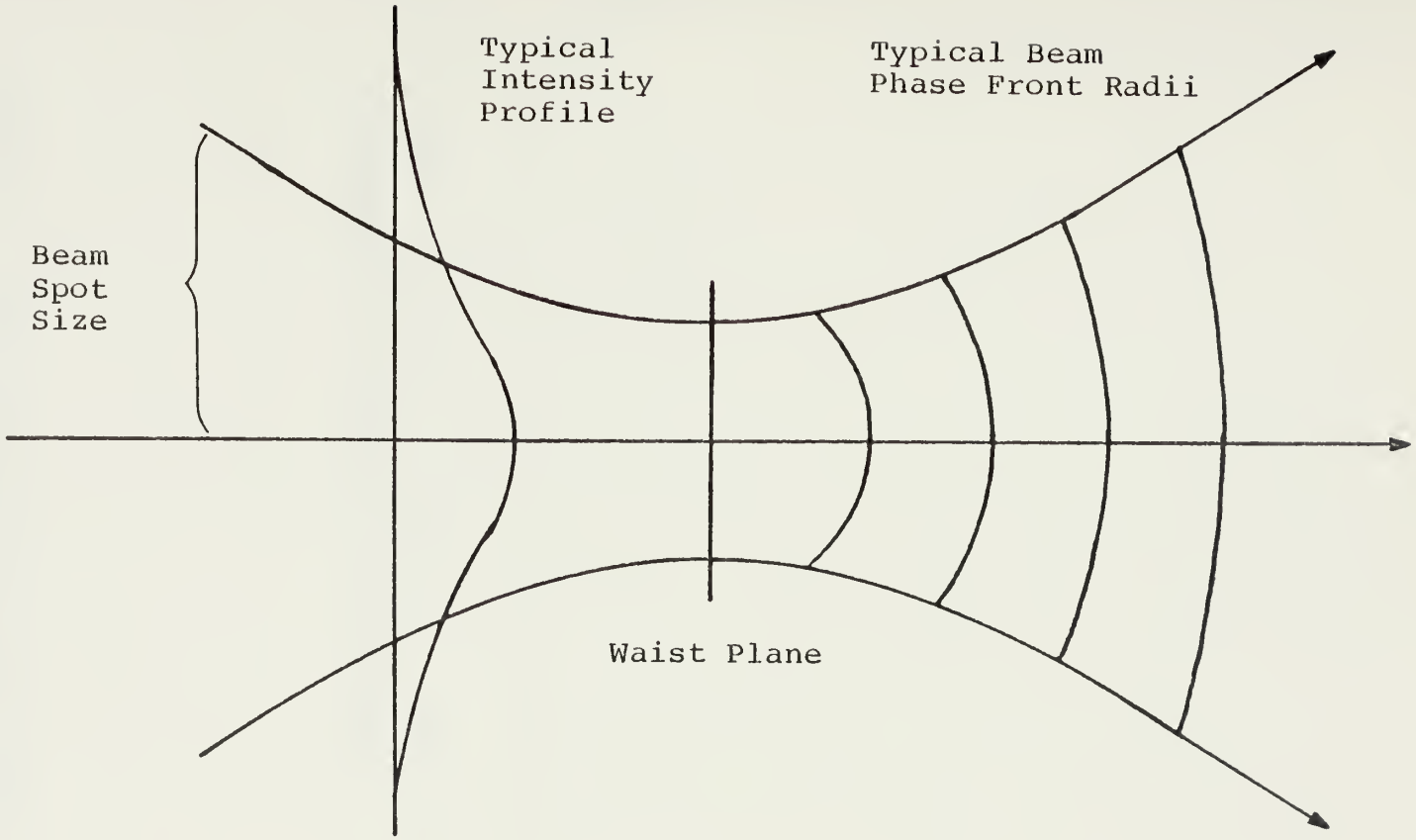

Figure 2. Gaussian Beam Characteristics

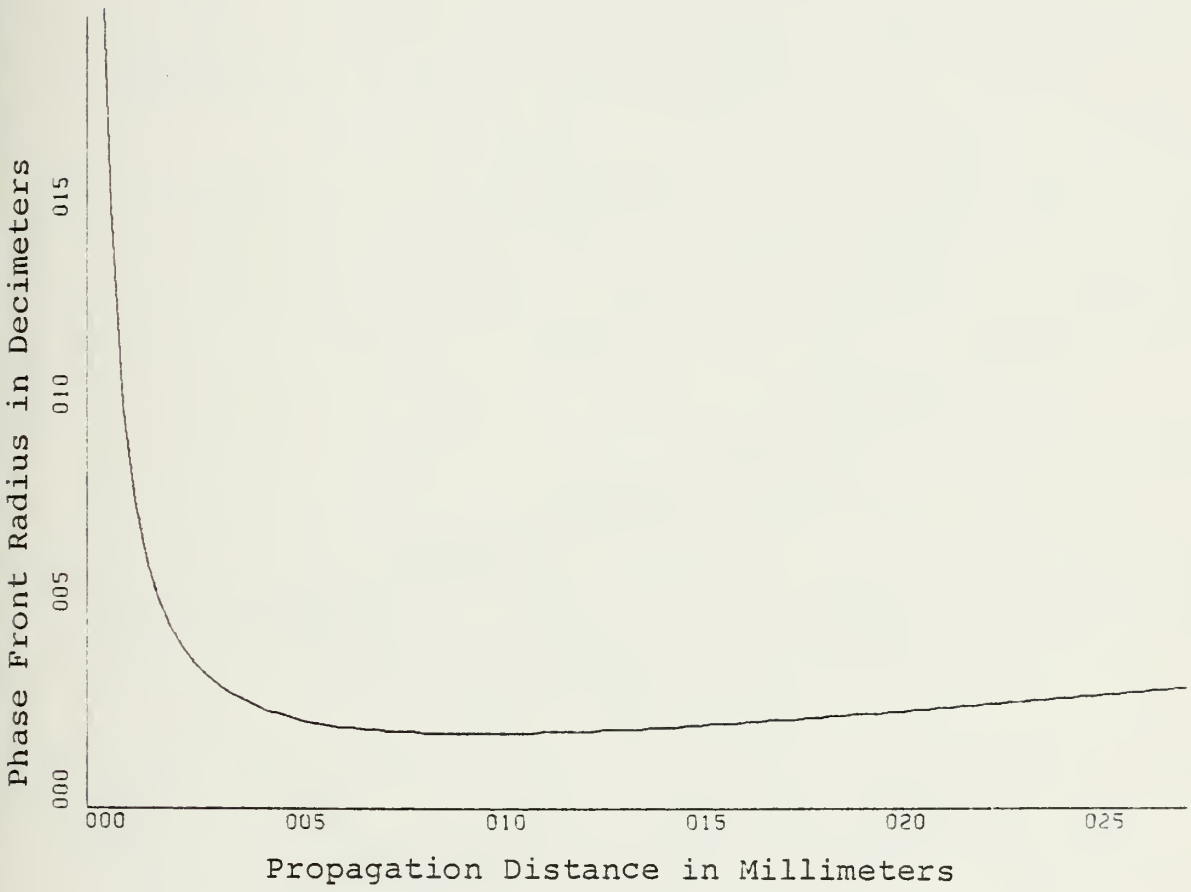

Figure 3. Phase Front Radius as a Function of Propagation Distance

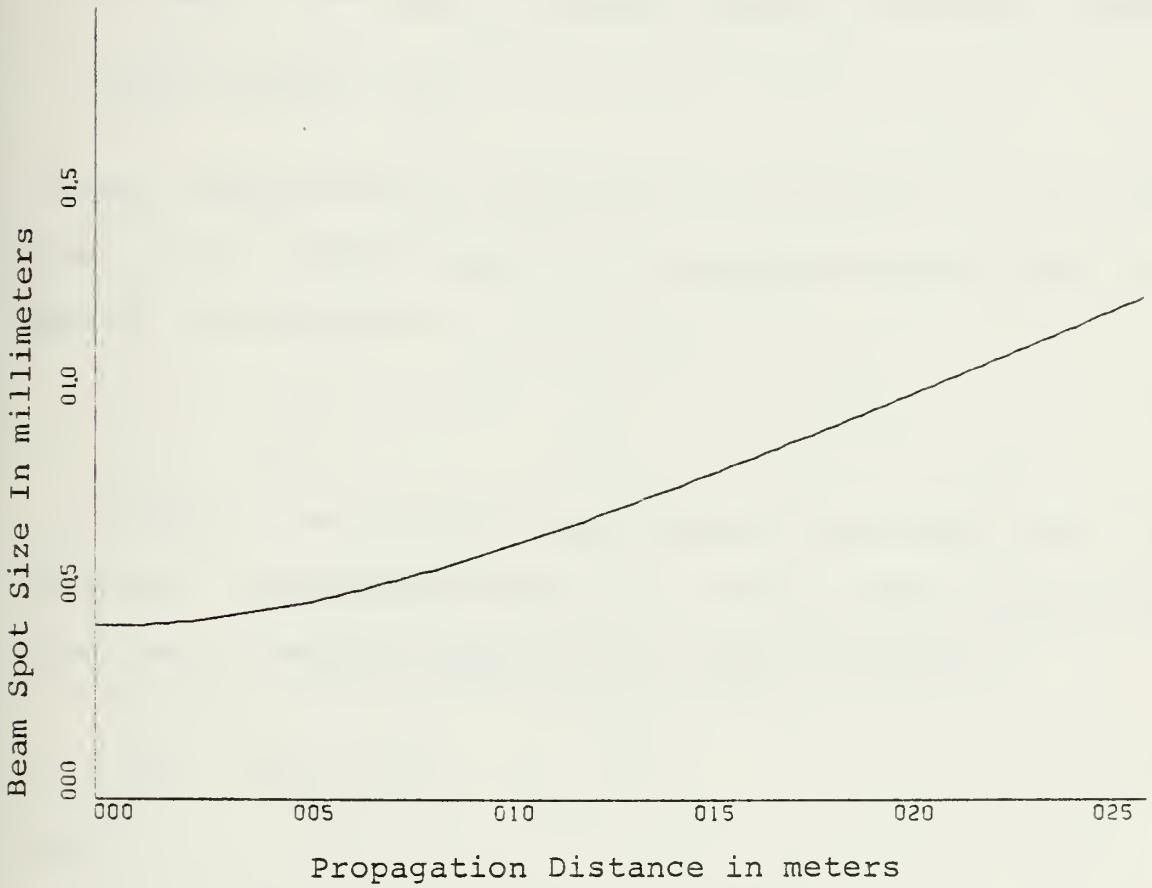

Figure 4. Beam Spot Size as a Function of Propagation Distance

In order to predict beam behavior through a thin lens, the quantity q must be introduced. This value is known as the 'complex beam radius'. It is defined by the following relation.

$$\text{Complex Beam Radius} = 1/q(z) = 1/R(z) - j\lambda/\pi w^2(z) \quad (3)$$

At the waist, the beam radius R(0) goes to infinity, leaving:

$$q(0) = j\pi w_o^2/\lambda = q_o \quad (4)$$

Patient manipulation of Equations (1) through (4) will yield Equation (5), which completely describes Gaussian beam transmission in free space.

$$q(z) = q_o + z \quad (5)$$

Spherical waves which pass through thin lenses obey the lens law. For Gaussian beams, the complex beam radius undergoes the following transformation shown in Figure 5.

$$1/q_2 = 1/q_1 - 1/f \quad (6)$$

where:

q_1 = incident beam's complex radius

q_2 = exit beam's complex radius

f = thin lens focal length

The above equations provided the basis for the TI-58 or TI-59 hand-calculator program to deal with Gaussian beam propagation through free space and thin lenses. This program is listed and explained in Appendix B. The first practical application of the program was to compute the beam spot size incident to the image plane photodetector array of an

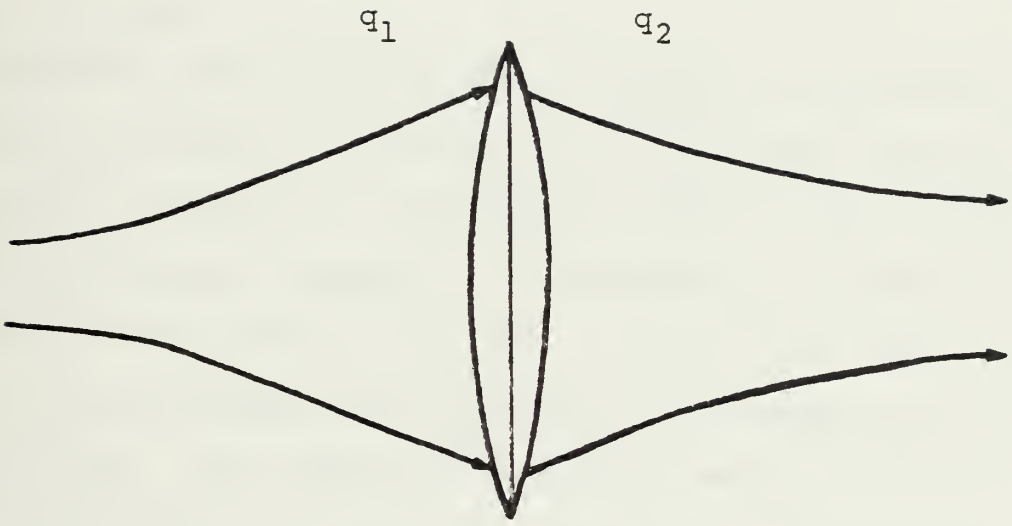

Figure 5. Gaussian Beam Transiting Thin Lens

experimental acoustooptic spectrum analyzer constructed as part of this work effort.

The calculation's accuracy was dependent upon one primary assumption. The beam profile could not be significantly truncated by the Bragg cell aperture or any of the thin lenses in the beam path. This assumption was adequately justified for the lenses used. A lens diameter of three times the spot size is sufficient to contain 99 percent of the beam power. All lenses in the experimental set-up were greater than five spot sizes wide.

However, this criterion was not upheld as the beam passed through the Bragg cell aperture. The beam spot size was expanded to completely illuminate the aperture and thereby enhance information capacity. Consequently, the beam profile was substantially truncated. In the limit, the incident beam cross-sectional intensity would have become uniform in distribution. The resulting exit beam, were it produced by the interaction of a plane sound wave and a rectangular light aperture of finite dimensions, would have had a horizontal intensity profile given below by Equation (7). This formula is based on the Fraunhofer approximation and is derived in Ref. 17.

$$I(r,\theta) = I_o(r) \left\{\frac{\sin\{\lambda D\theta/\lambda\}}{\{\pi D\theta/\lambda\}}\right\}^2 \qquad (7)$$

where:

$I(r,\theta)$ = Intensity as a function of angle off the Bragg cell aperture boresight and path length to the image plane

$I_o(r)$ = Boresight light beam intensity

D = Aperture horizontal dimension

λ = Laser wavelength

θ = Angle off boresight

r = Distance to transform lens

The $1/e^2$ beamwidth was determined from Equation(7) by an iterative algorithm. The solution is given by Equation (8).

$$\text{Sinc Function } 1/e^2 \text{ Beamwidth} = SBW = 1.4r\lambda/D \qquad (8)$$

In order to determine the seriousness of violating this criterion, beamwidth calculations were made for both extremes. The first assumed an incident Gaussian beam with no truncation. The second assumed an incident plane wave. Results of the calculations were compared with an experimentally determined value.

The equipment used to make confirming observations of image plane beam spot size is block diagrammed in Figure 6. Component devices are described in the following paragraphs, and dimensional quantities needed by the propagation program are provided in Table I.

The laser utilized for the measurements was a Spectra-Physics 115. It produced a .5 milliWatt continuous wave output which had a TEM_{oo} spatial mode and random polarization. Power line ripple and random noise contributions were limited to one quarter percent of the output power. The longitudinal mode spacing was 550 MHz.

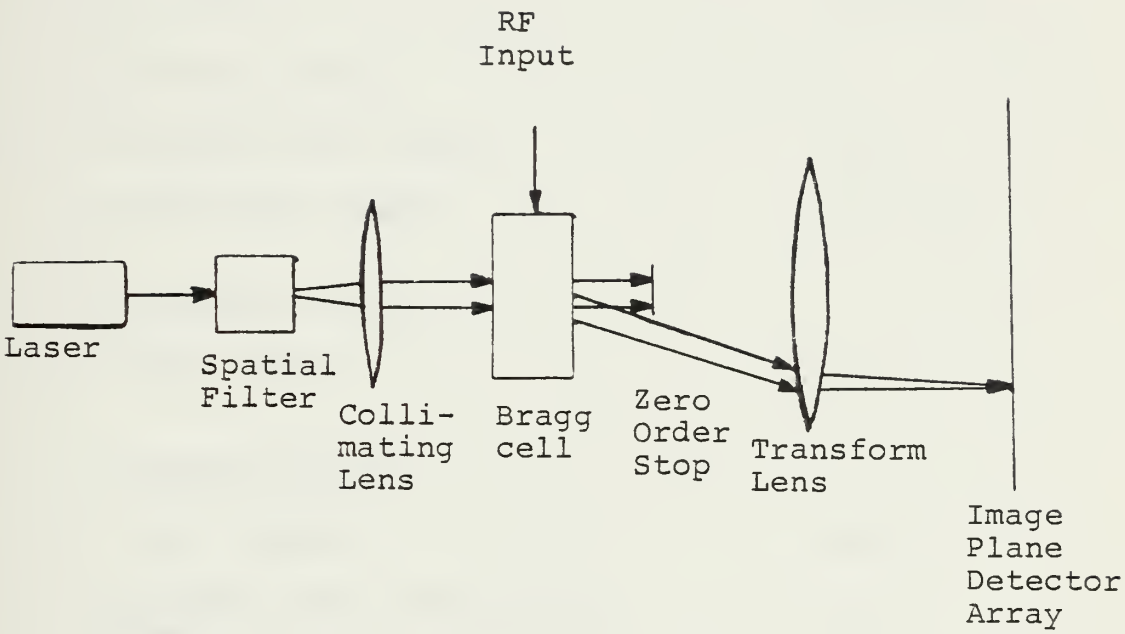

Figure 6. Experimental Acoustooptic Spectrum Analyzer

TABLE I. PROPAGATION PROGRAM INPUTS

LASER	
EXIT BEAM SPOT SIZE	.44 mm
EXIT BEAM RADIUS	INFINITY
WAVELENGTH	.6328 um
SPATIAL FILTER	
DISTANCE FROM LASER	.1 m
LENS FOCAL LENGTH	14.8 mm
COLLIMATING LENS	
FOCAL LENGTH	.254 m
TRANSFORM LENS	
FOCAL LENGTH	.304 m
DISTANCE FROM COLLIMATING LENS	.3 m

A spatial filter followed the laser in the operating train sequence. It removed intensity fluctuations which were due to light scattering from the beam profile. Dust on the laser windows and output mirrors is the major cause of this disturbance, although lens imperfection may be a contributing factor as well.

The spatial filter performed its cleaning task by focusing the beam through a small pinhole. This focusing action caused the scattered light to spread out from the central beam. Light remaining in the central beam had a smoothed Gaussian profile. The pinhole passed the major portion of the central beam and removed the scattered light. Slight truncation of the beam by the pinhole produced an Airy Disk diffraction pattern. This phenomenon is discussed by Born and Wolf in Ref. 18.

The outer rings of the Airy pattern were removed by passing the central beam through a second aperture or iris. The net far field beam profile had a nearly ideal Gaussian shape. This beam was collimated by a thin lens. Doing so ensured complete illumination of the succeeding Bragg cell aperture.

The particular Bragg cell employed in this set up was an Isomet (1205-1-2). It used Lead Molybdate ($PbMoO_4$) as the interaction medium. The bandpass center frequency was 80 MHz. This translated to a deflection angle of 7 milliradians. Nominal rf input power was one and a half Watts.

An 80 MHz, fixed amplitude, continuous sine wave was chosen as the input drive signal. A pure sinusoidal tone was used so that no part of the measured beamwidth was due to the input

signal. The deflected beam was assumed to be a function only of the interaction between the Gaussian light beam and the Bragg cell aperture's size and shape. Discussion of profile affecting light-sound interplay is delayed until the next section.

When the Bragg cell was excited by the input signal, two light beams exited the device orifice. The first beam or "zero order diffraction beam" was not deflected. The only information carried by it was in the form of amplitude modulation. A stronger input signal would have meant a weaker undeflected beam. This beam was not useful and therefore terminated by a opaque zero order stop. The second beam was deflected, and represented first order diffraction. It was passed through the transform lens and brought to a focus on the image plane linear detector array for width measurement.

The transform lens played either one of two different roles which depended upon whether the diffracted beam had a Gaussian or Sinc function intensity profile. If the beam were truly Gaussian and still well collimated as it exited the Bragg cell, then the image plane spot size would have been insensitive to changes in the distance between Bragg cell and the transform lens. The important distance which needed precise calculation would have been that from the lens to the image plane. In the case of a well collimated Gaussian beam, this span is nearly equal to the lens focal length.

Conversely, had the exit beam exhibited a Sinc function intensity profile, then the distance from the lens to the image plane would have been arbitrary. Such a beam would

have appeared to emanate from a point source at the Bragg cell aperture. A thin lens positioned a focal length away would have collimated the beam. The resulting spot size, as shown in Equation (7), would have been a function only of the distance to the transform lens, and not of the transform lens-image plane separation.

The observed image plane spot size was sensitive to changes in either separation distance. This result implied the exit beam had retained characteristics of both profiles. The optimal transform lens position was located approximately one focal length away from the Bragg cell and a focal length from the image plane. This "best arrangement" is confirmed by Whitman and his associates in Ref. 19.

The image plane sensor used to detect beamwidth was a (CCD121H) linear detector array developed by Fairchild. It consists of 1728 sensor elements and is a charge coupled, buried channel device. The output is delivered serially and, for the experiment, went to a Tektronics 422 oscilloscope display. A typical output display, which resulted from an 80 MHz monotone input signal, is shown in Figure 7.

The physical apportionment of the photo elements is shown in Figure 8. The $1/e^2$ beamwidth was measured by expanding the oscilloscope time display and counting photosite output peaks within the beamwidth. This number was converted into a spatial dimension by using the known dimensions in Figure 8.

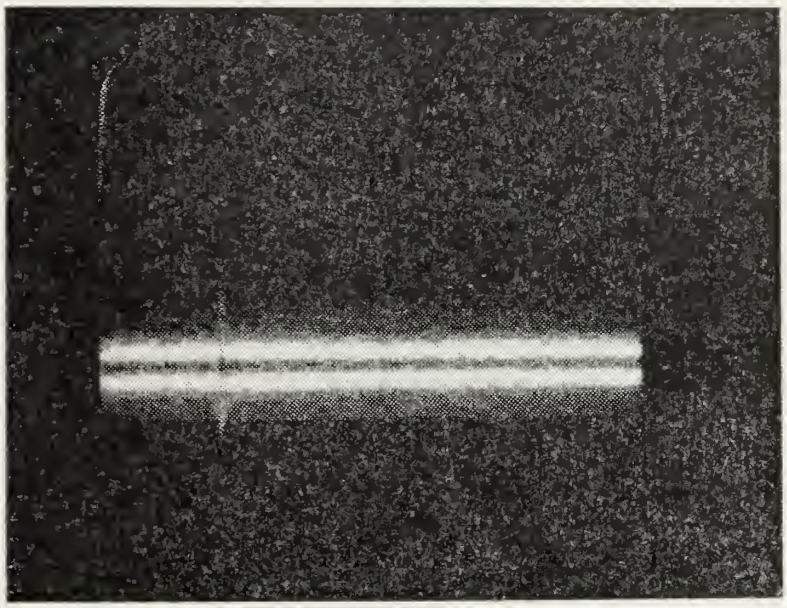

Figure 7. Photodetector Array Output

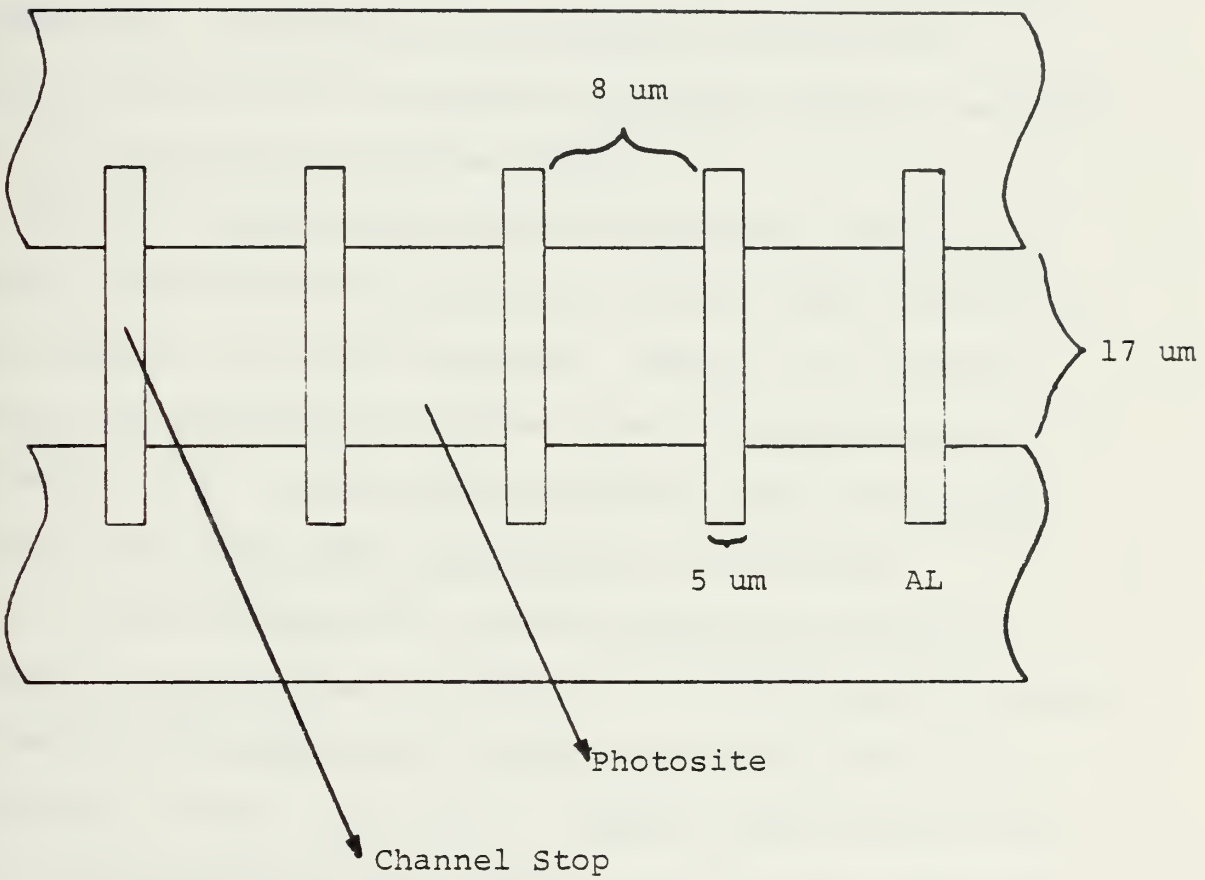

Figure 8. Photo Element Dimensional Diagram

The Sinc profile was determined using Equation (8) and the following values:

r = focal length of transform lens = .304 m

λ = Helium-Neon Laser wavelength = .6328 um

D = effective aperture width = .7 cm

The Gaussian beamwidth was calculated by using the propagation program and Table I. Intermediate results are listed in Table II. Incidently, this table may be used as a standard solution set to ensure all proper entries are keyed into the calculator's program memory.

Table III compares the three independently determined values. These results indicate the actual beam profile was very similar to the Sinc function. However, the highest sidelobe was measured 17 dB down from the central peak. If the profile were an ideal Sinc function, then the highest sidelobe would have been approximately 14 dB down.

D. L. Hecht presented a concise sidelobe analysis of truncated Gaussian beams in Ref. 20. In one graph he related the maximum sidelobe level to beam truncation ratio- D/2w. This graph is shown in Figure 9. Again, this does not take into account effects of the sound column of the light beam profile, it is a function only of truncation ratio.

Figure 9 provided a rough means of indirectly determining truncation ratio. For a -17 dB sidelobe, the corresponding truncation ratio was in the range of .55 to .6. The actual truncation ratio value was calculated as .47. It was determined by using the spot size given in Table II for the beam

TABLE II. BEAM PROFILE INTERMEDIATE RESULTS

At Laser Aperture

Beam Spot Size = w = .44 mm
Beam Radius = R = ∞

After propagating .1 m

w = .4424 mm
R = 9.377 m

At Spatial Filter Lens Exit

w = .4424 mm
R = -14.82 mm

After propagating 14.820044 mm

w = 6.749 um
R = ∞

After propagating .254 m

w = 7.581 mm
R = .2540

At Collimating Lens Exit

w = 7.581 mm
R = -3.205×10^{5} m

After propagating .3 m

w = 7.581 mm
R = 1.770×10^{6} m

At Transform Lens Exit

w = 7.581 mm
R = -.3040 m

After propagating 3.039997 m

w = 8.077 um
R = ∞

TABLE III. COMPARISON OF BEAMWIDTH VALUES

Sinc Image Plane Beamwidth	38 um
Measured Image Plane Beamwidth	34 um
Gaussian Image Plane Beamwidth	16 um

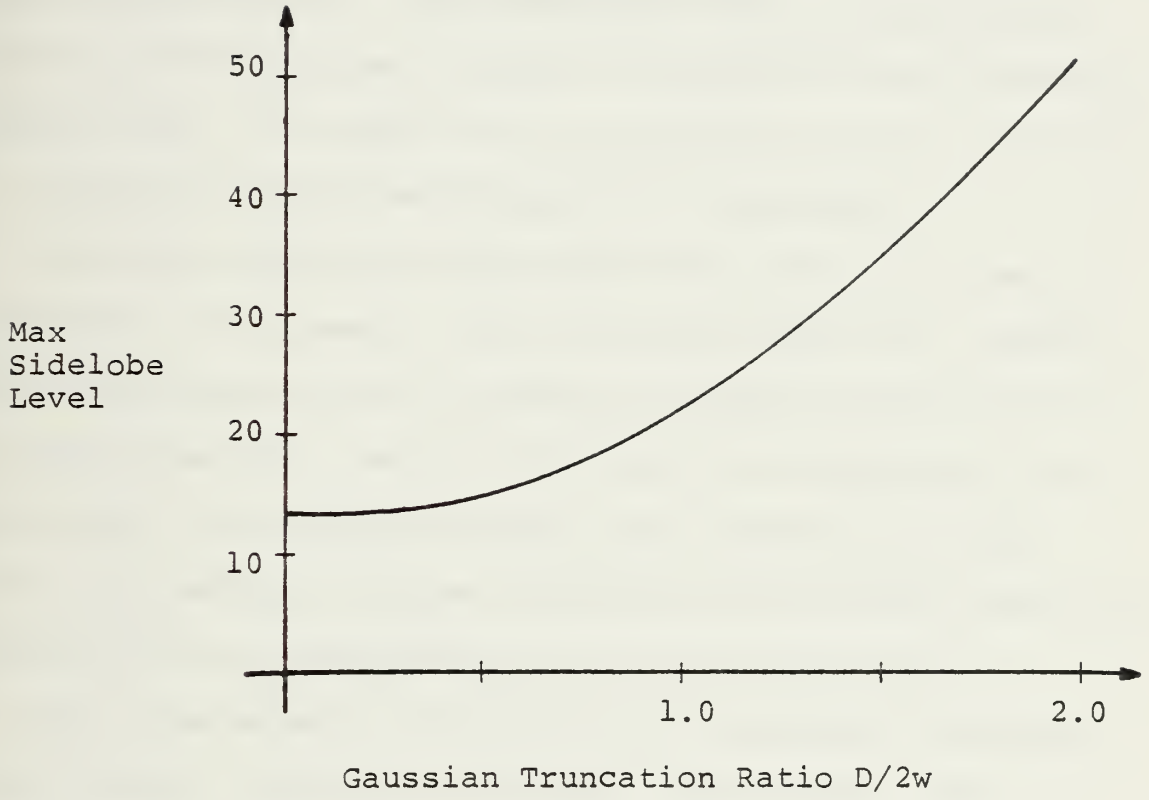

Figure 9. Maximum Sidelobe Level vs Trancation Ratio

entering the Bragg cell (.75 cm) and the deflector aperture width (.7 cm). The graph determined value differed by 17 percent.

This disagreement is not very surprising in view of possible sound column effects and other error sources. Channel stops were believed to have played a role in limiting precision measurements. The intervening metal strip between two adjacent photosites consumes 24 percent of the available surface area. Its effect can be minimized but not eliminated by "rocking" the diffracted beam back and forth.

Lack of a precision focus could have also distorted observations. If present, minor lens and Bragg cell imperfections would have slightly affected ultimate focusability of the beam, however, operator error was not particularly suspect here. Even though focusing was a tedious exercise, minor lens position changes produced very noticeable amplitude deviations in an expanded scale oscilloscope display.

Also, the detector array was not a perfectly one-dimensional sensor. Each pixel averaged the incident light intensity over a rectangular area. The vertical photosite dimension was twice the magnitude of the horizontal. It was also equal to the main lobe beamwidth calculated for an ideal Gaussian beam. It is not fair to assume that the ratio of averaged intensities would have necessarily been identical to the ratio of the peak values. A closer ratio agreement would have been realized with a smaller vertical dimension.

The subject of diffraction beam sidelobe effects is the last remaining topic of this section. D. L. Hecht [22] has

shown a way to anticipate sidelobe levels, but no one, to this author's knowledge, has specifically addressed sidelobe suppression. The obvious approach of increasing the truncation ratio to suppress sidelobes has the previously mentioned drawback of reduced information capacity. In present systems having only 30 dB overall dynamic range, a -20 dB maximum sidelobe level may not be significantly harmful. However, wider dynamic ranges in newer systems are now evident, so eventually the problem must be confronted.

Since spatial sidelobes are a direct result of the abrupt windowing action by the aperture, the only way to remove them is by making the absorption-transmission changeover a less discontinuous process. To produce a smoother window function, a graded film mask could be deposited on the deflector aperture exit. Or, absorptive impurities could be diffused into the interaction medium to produce the same effect. The absorption profile would only need to be a function of the horizontal axis as vertical sidelobes do not interfere normally in a one dimensional array. Figure 10 depicts a possible graded transmission profile which exhibits a smooth transition from infinite to zero attenuation.

This completes the formal discussion on laser beam propagation. To recapitulate, a brief review of propagation characteristics was presented. Behavior-determining equations explained in the review were utilized in a calculator program for beam spot size and radius prediction. Gaussian beam model results were compared with experimentally observed figures and those predicted by a plane wave-aperture interaction model.

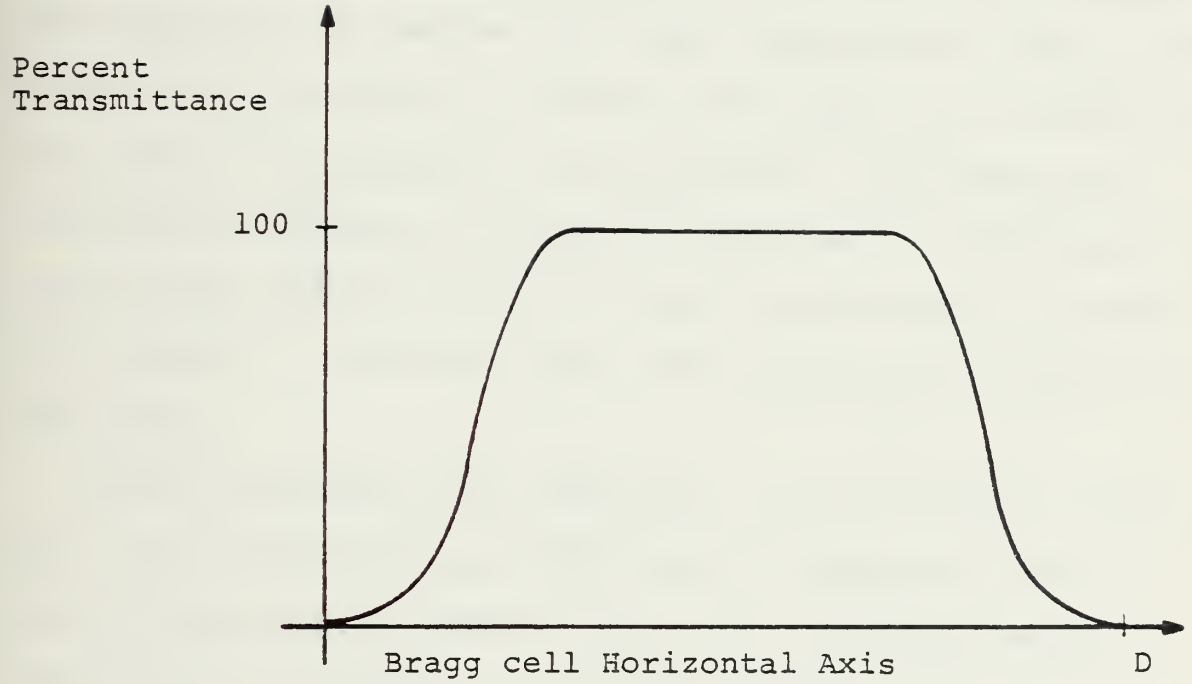

D = Aperture Width

Figure 10. Graded Transmittance Profile

Truncation ratio was found to play a dominant role. Finally, the significance of sidelobe interference was discussed and two methods of sidelobe suppression were suggested.

C. BRAGG CELL PERFORMANCE

As mentioned in the introduction, a Bragg cell translates a time domain signal into the frequency domain by converting a signal's component frequencies into beam deflection angles, and respective intensities into beam intensities. This process is sketched in Figure 11. How well the Bragg cell accomplishes this task is the subject of this section. The three major performance criteria of diffraction efficiency, information capacity and response time were used to partition the investigation effort. The first topic under analysis was diffraction efficiency.

Before beginning this discussion, a brief mention of the basic law governing Bragg deflection is required. This is given by Equation (9) which relates the deflection angle to the acoustic wavelength of the input signal.

$$\frac{\lambda_o}{2\Lambda_o} = \sin\theta \simeq \theta \tag{9}$$

or

$$\theta = \frac{\lambda_o f}{2v}$$

where:

λ_o = laser wavelength

Λ_o = acoustic wavelength

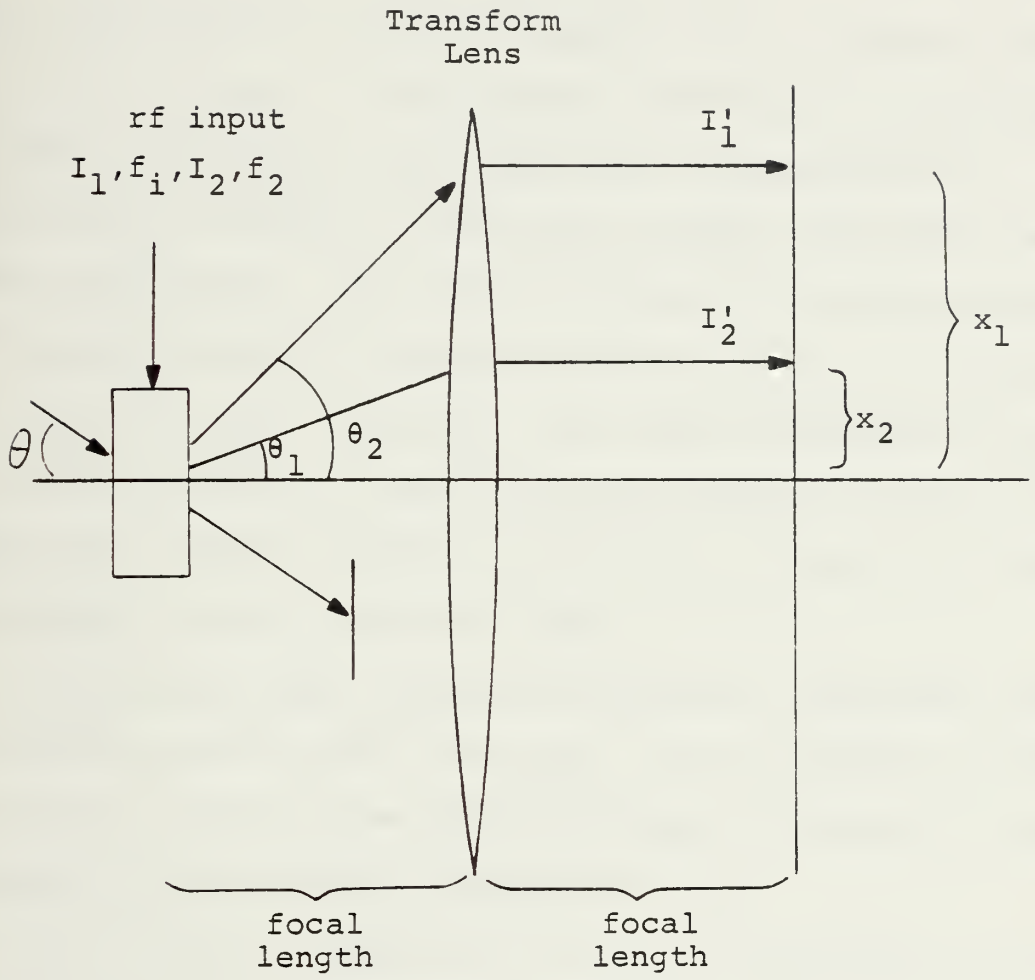

$x_1 \simeq f_1 \theta_1$ $\quad I_1' = \eta_1 I_1$ $\quad \eta_x$ = Net Efficiency

$x_2 \simeq f_2 \theta_2$ $\quad I_2' = \eta_2 I_2$ $\quad \eta_1 = \eta_2$

Figure 11. Bragg cell Operation

θ = deflection angle

f = input frequency

V = acoustic velocity

A detailed geometric proof of Equation (9) is given by Yariv in Ref. 13. Since θ is very small, typically on the order of seven milliradians, the first order approximation is sufficiently accurate for spectrum analyzer and optical excisor applications. Only the two factors of laser wavelength and acoustic velocity are able to alter the ratio of deflection angle to input frequency. The laser wavelength is chosen from those available to best match the transmittance of the Bragg cell, and the acoustic velocity is a function of other constraints, as will be shown later.

On the other hand, the beam diffraction efficiency has many factors which affect its value. This parameter is defined as the ratio of the diffracted beam intensity to the intensity of the original undeflected beam.

This is shown in Equation (10) which determines the ratio. It was derived by I. C. Chang in Ref. 21.

$$\frac{I_1}{I_o} = \eta \frac{\sin^2 \{\eta + \{\Delta K_1 L/2\}^2\}^{\frac{1}{2}}}{\{\eta + \{\Delta K_1 L/2\}^2\}} \tag{10}$$

with

$$\eta = \frac{\pi^2}{2\lambda_o^2} \left(\frac{n^6 p^2}{\rho V^3} \right) \frac{P_a L}{H \cos^2 \theta_o} \tag{11}$$

where:

I_1 = diffracted beam intensity

I_o = original undeflected beam intensity

λ_o = free space laser wavelength

n = refractive index

p = elastooptic coefficient

ρ = mass density

V = acoustic wave velocity

P_a = acoustic power

L = interaction length

H = acoustic beam height

ΔK_1 = wavevector mismatch

θ_o = deflection angle determined from equation (9)

An approximate version easier to work with is given by Equation (12):

$$\frac{I_1}{I_o} = \sin^2\{\eta^{1/2}\} \frac{\sin^2\{\Delta K_1 L/2\}}{\{\Delta K_1 L/2\}^2} \qquad (12)$$

Let:

$$A = \sin^2\{\eta^{1/2}\}$$

$$B = \frac{\sin^2\{\Delta K_1 L/2\}}{\{\Delta K_1 L/2\}^2}$$

Term A of equation (12) is constant with respect to input signal frequency. Its effect will be examined later. Term B fixes the relative bandshape of a normal acoustooptic beam

deflector. By converting wavevectors to frequencies, B may be expressed as:

$$B = \frac{\sin^2\{\pi/2L/L_o\{FF_m - F^2\}\}}{\{\pi/2L/L_o\{FF_m - F^2\}\}^2} \tag{13}$$

where:

F = normalized center frequency = 1

F_m = input frequency normalized to the center frequency value

$L_o = n\Lambda_o^2 \cos\theta_o/\lambda_o$ = characteristic interaction length

This transformation is shown by D. L. Hecht in Ref. 20. A plot of this equation with various ratios of L/L_o is shown if Figure 12. The 3 dB bandwidth is given by equation (14) and is also from /20/.

$$\Delta f = 1.8 f_o L_o / L \tag{14}$$

where:

f_o = center frequency

Equations (10) through (13) describe Bragg regime or "thick grating" diffraction. Only a first order beam will be deflected with a thick diffraction grating. A thin diffraction grating will yield many higher order diffraction beams in addition. This type of diffraction is referred to as Raman-Nath diffraction. It is intolerable for the intended applications because of interference caused by the additional beams.

Equation (14) implies that the deflector bandwidth can be easily increased by shortening the interaction length.

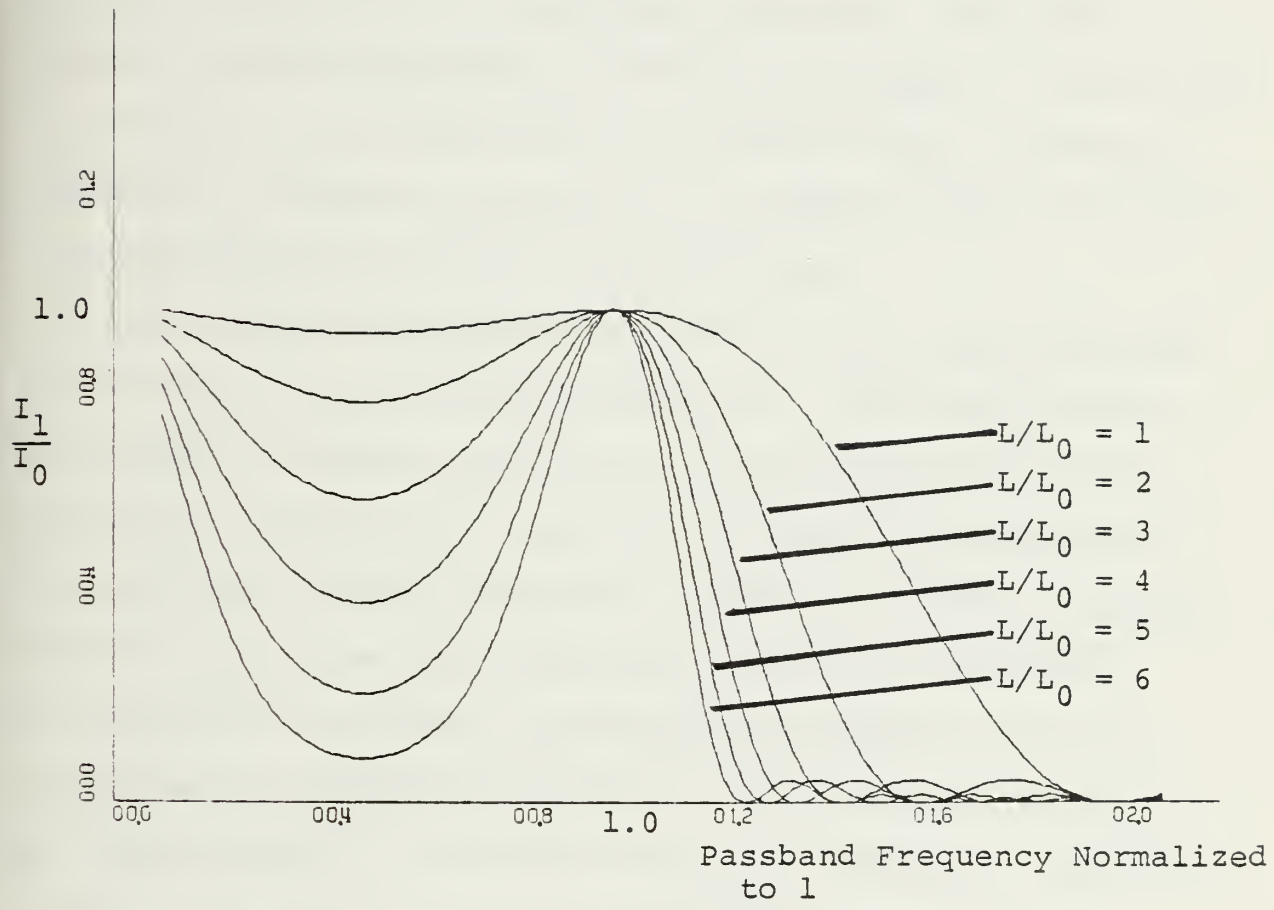

I_0 = Intensity of Diffracted Beam at Center Frequency

I_1 = Intensity of Diffracted Beam at Arbitrary Frequency

Figure 12. Diffraction Efficiency Bandshape

Increasing bandwidth in this manner is of limited overall benefit as the diffraction shifts from the Bragg regime to Raman-Nath. In general, normal Bragg diffraction is restricted to one octave.

This leaves only one effective way in Equation (14) to enlarge the Bragg cell's operating bandwidth. The input signal's center frequency, f_o, must be increased. The ability to increase f_o is determined by the input signal transducer. Substantial transducer analysis is included in Refs. 10 and 21. The highlights are briefly presented here.

The acoustic transducer consists of a thin piezoelectric strip bonded to the interaction medium. Its effectiveness in launching an acoustic wave into the interaction medium is a function of coupling and impedence matching characteristics. The particular bonding technique bounds the maximum frequency that the transducer can effectively couple to the medium. The degree of electrical and mechanical impedence matching determines the transfer efficiency from electrical to acoustical signal energy. It is also frequency dependent. Reference 2 reports some available deflectors which operate in the three to four Gigahertz region.

The above discussion of tranducer effects completes the analysis of Equation (12)'s term B. Attention is now directed to term A. It relates the interaction medium's material constants to diffraction efficiency.

The argument of term A may be rewritten as:

$$\eta^{\frac{1}{2}} = \frac{\pi}{2} \cdot C \tag{15}$$

where:

$$C = \left\{\frac{\sqrt{2}}{\lambda_o} \frac{n^3 p}{\sqrt{\rho} V^{3/2}} \sqrt{\frac{P_a L}{H} \cdot \frac{1}{\cos\theta_o}}\right\} < 1 \tag{16}$$

Since $\eta^{\frac{1}{2}}$ is a sine function argument, improvement in diffraction efficiency is a "simple" matter of increasing C. It is desirable to increase the refractive index - n and elastooptic coefficient - p, and decrease the acoustic beam height H, the acoustic velocity - v and the mass density - ρ. Little can be done with λ_o, $\sqrt{2}$ or θ_o. Also, the deleterious effects of increasing acoustic input power have been noted in the introduction. And, inordinate increasing of L would prove costly in terms of bandwidth by Equation (14).

Several acoustooptic figures of merit have gained acceptance for use in the selection of suitable interaction mediums. They are:

$$M_1 = \frac{n^7 p^2}{\rho V} = M_2\{nV^2\} \tag{17}$$

$$M_2 = \frac{n^6 p^2}{\rho V^3} \tag{18}$$

$$M_3 = \frac{n^7 p^2}{\rho V^2} = M_2\{nV\} \tag{19}$$

$$M_4 = \frac{n^8 p^2 V}{\rho} = M_2\{nV^2\}^2 \tag{20}$$

Gordon introduced M_1 and M_2 in Ref. 22. His results were further clarified by Chang in Ref. 21. Chang also included a discussion of M_3 and M_4. M_1 in equation (21) related diffraction efficiency to acoustic power for a given bandwidth. This is yielded by Equations (11), (14) and (17).

$$\frac{\eta}{P_a} \approx \frac{M_1}{\Delta f}\left\{\frac{9}{\lambda_o^3 f_o H}\right\} \tag{21}$$

where:

$$9 \approx 1.8\pi/2$$

This same efficiency-power ratio can be expressed in terms of a fixed geometry by using M_2 in Equation (21).

$$\frac{\eta}{P_a} \approx M_2\left\{\frac{L}{H}\right\} \cdot \left\{\frac{5}{\lambda_o^2}\right\} \tag{22}$$

M_3 is the preferred figure of merit for systems in which the transducer height is not limited by impedence or fabrication constraints. H would then be limited only by the laser beam height entering the cell. For convenience, H is replaced by $V/\Delta f$, which transforms Equation (21) into Equation (23).

$$\frac{\eta}{P_a} \approx M_3\left\{\frac{9}{\lambda_o^3 f_o}\right\} \tag{23}$$

where:

$$P_d = P_a/LH \tag{25}$$

In addition to having high values of the above figures of merit, a good interaction medium should exhibit other characteristics as well. Low coefficients of optical and acoustic attenuation are desirable. Optical attenuation degrades overall performance and ocntributes heat to the material. Acoustic attenuation decreases information capacity. Lastly, if the material is crystalline, then consideration must be given to how easily a continuous crystal structure can be pulled from a melt. For specific information on medium performance, see Ref. 10 which contains an extensive comparison of material properties.

Once the deflector material has been chosen and the device dimensions fixed, nothing remains free in Equation (10) to improve diffraction efficiency except for the acoustic input power. However, beam steering and other compensation techniques can still be called upon to improve performance more. Korpel's work [5] on stepped transducer beam steering has already been briefly cited. Gordon [22] also discussed beam steering, only with a planar instead of stepped array. Both transducers represented first order steering as each successive element differed in phase by π radians.

Pinnow [23] compared normal or single transducer element Bragg diffraction with stepped and planar first order beam steering. He argued effectively that beam steering was better as it required less total acoustic power and a lower cell

acoustic power density. This is shown most clearly by attempting to double bandwidth in a single element deflector cell by doubling center frequency. The effects are revealed in Equation (14) with L_o rewritten in terms of frequency.

$$L_o = n\Lambda_o^2 \cos\theta_o/\lambda_o = \{\frac{\eta}{\lambda_o}\cos\theta_o\}\{\frac{V^2}{f_o^2}\} = K\{\frac{V^2}{f_o^2}\} \tag{26}$$

$$f = 1.8 f_o L_o/L = 1.8 f_o K\{\frac{V^2}{f_o^2 L}\} \tag{27}$$

Doubling the bandwidth by doubling f_o causes the transducer length to reduce to one quarter as shown in Equation (28).

$$2\Delta f = \{1.8\}\{2f_o K\}\{\frac{V^2}{4f_o^2 L/4}\} \tag{28}$$

This occurrence induces the acoustic power from Equation (22) to quadruple.

$$\frac{\eta}{4P_a} \approx M_2\{\frac{L/4}{H}\}\{\frac{5}{\lambda_o^2}\} \tag{29}$$

The net result is four times the original acoustic power is spread over one fourth of the original surface area. Pinnow explained how this unhappy conclusion could be largely circumvented by using a first order array of only moderate complexity.

To begin, he pointed out that a stepped transducer array is nearly twice as efficient as a planar array. A first order

planar array must divide its power between two beams which are symmetric about the normal. The corresponding stepped array utilizes its inherent asymmetry to put a large percentage of the acoustic power into a single main lobe. A typical first order stepped array is depicted in Figure 13.

The performance improvement provided by a stepped array was calculated in terms of an effective acoustic power ratio. To accomplish this, the array beam pattern needed to be determined. For simplicity, it was described in terms of far field approximations even though the light-sound interaction actually takes place in the near field. The overall pattern was taken to be the produce of the single element and array functions.

(18) $$W(\theta) = B(\theta)C(\theta) \tag{30}$$

where $B(\theta)$ is defined as the single element function and is given by

$$B(\theta) = \left\{ \frac{\sin\{\frac{\lambda L \theta}{\Lambda}\}}{\{\frac{\lambda L \theta}{\Lambda}\}} \right\}^2 \tag{31}$$

$C(\theta)$ is the array function and is

$$C(\theta) = \frac{\sin^2\{\frac{N\pi D}{\Lambda}(\theta-\theta')\}}{\frac{N D}{\Lambda}(\theta-\theta')^2} \tag{32}$$

θ' = beam steering angle

θ = angle from normal to element plane

D = center to center element spacing

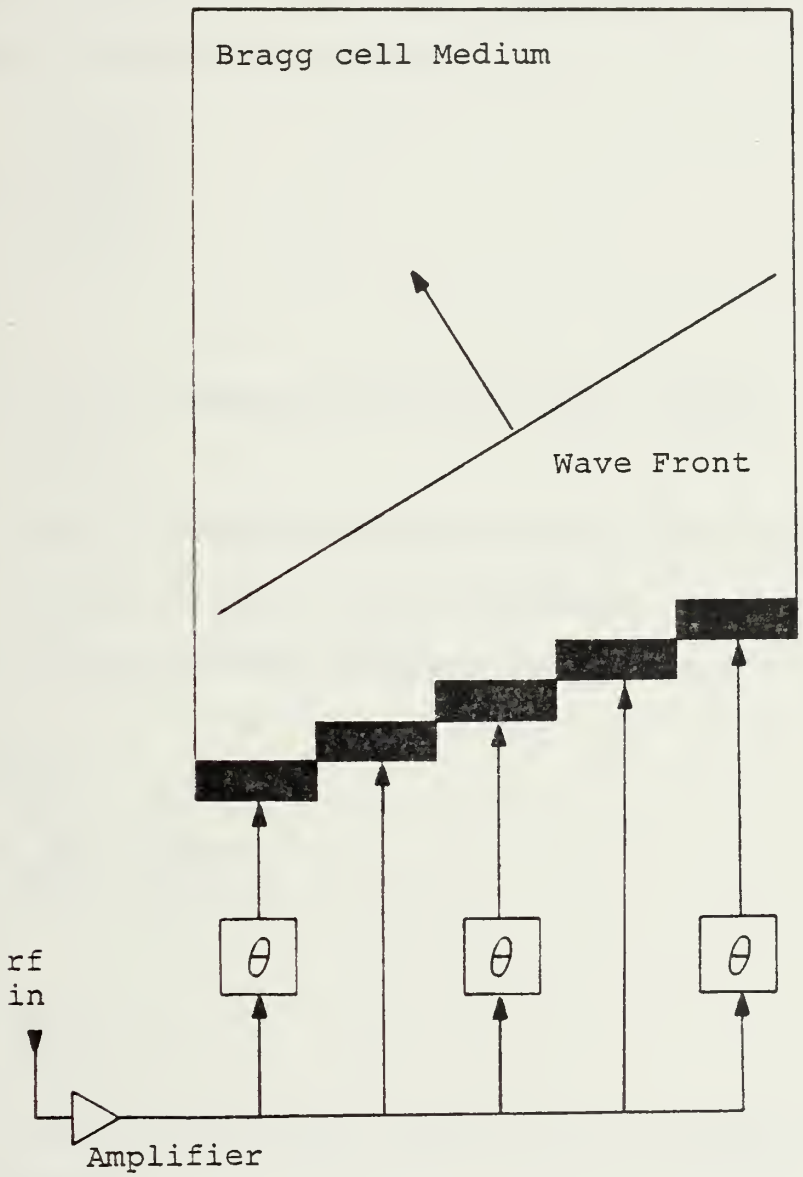

Figure 13. First Order Stepped Array

L = element length

N = number of transducer elements

The array performance was compared at midband with a deflector having one element of length L_o by taking the ratio α of the effective array beam power over the effective single element transducer beam power.

$$\alpha = \frac{P_b' L W_a}{P_a' L_o W_s} \tag{33}$$

where:

P_b' = Array Acoustic Power per unit lingth

$= P_a'/N$

P_a' = Unit Transducer Beam Power per unit length

W_a = Array Pattern value at midband

W_s = Single Element Pattern at midband $\simeq 1$

This leaves

$$\alpha = \frac{W_a L}{N L_o} = \frac{W_a}{N^2} \beta \tag{34}$$

where:

$\beta = NL/L_o$

is the ratio of the array length to the single element transducer lengths.

At midband:

$$B(\theta) = G < 1 \tag{35}$$

$$C(\theta) = N^2 \left\{ \frac{\sin\left\{\frac{\lambda D}{\Lambda}\{\theta-\theta'\}\right\}}{\sin\left\{\frac{\lambda D}{\Lambda}\{\theta-\theta'\}\right\}} \right\}^2 \tag{36}$$

$$\simeq N^2$$

therefore:

$$\alpha \simeq GN \tag{37}$$

The end result is a performance factor α equal to something less than the number of transducer elements. Pinnow did caution however, that increasing N much beyond four was self-defeating as the inherent errors of first order steering inhibit further improvement. Thus, first order beam steering can be utilized to provide some bandwidth improvement without increasing power. Its benefits must be subjectively weighed against the difficulties caused by increased device complexity.

Although beam steering does somewhat improve diffraction ratio consistency across the passband, there are also other optical and electrical techniques which can further minimize nonuniformities. A set of staggered bandpass filters inserted prior to the deflector could pre-distort the input signal to even out the humped midband response of a normal Bragg cell. This method would be amenable to both spectrum analysis and optical excision systems. If advantageous, an optical excisor could also employ post-distortion filtering equally as well, however, a spectrum analyzer would required a scheme of time varied gain for post-distortion. An optical filter or attenuator whose transmission is inversely related to the diffraction

ratio bandshape would be another possible contender. One method of obtaining such a filter employs photographic film as the filter medium. The technique tailors the component to a particular system by sweeping a single rf signal across the deflector passband while the resulting diffraction beam exposes an undeveloped film slide positioned between the deflector cell and photodetector. This film, once developed, would be a post-distortion filter and provide a uniform passband response, as portions of the film which were exposed to higher illumination intensities prior to development would attenuate the diffraction beam to a greater extent.

The analysis up to this point has assumed the deflector treats each rf signal frequency component independently of all others. This supposition is not entirely true as many secondary effects may be noticeably present. Each element of the composite input signal depletes the incident light beam's capacity to respond linearly to the other simultaneously present components. Diffracted beams may also be rediffracted by other acoustic wavefronts encountered prior to exiting the cell. D. L. Hecht [24] analyzed multiple frequency component effects. In order to do this, he used coupled mode equations to solve the classical wave equation, Equation (38), for N signals in both the Raman-Nath and Bragg regimes.

$$\nabla^2 E = \frac{\{u(x,t)\}^2}{C^2} \frac{\partial^2 E}{\partial t^2} \tag{38}$$

His solution algorithm is similar to that followed by Klein and Cook in Ref. 25. They, however, only treated the interaction

of a single frequency sound column with the incident light beam. Hecht's development and results for Bragg diffraction are discussed here as this type of interaction is more important for the intended applications.

The electric field E was represented as an N-dimensional Fourier series expansion which was much simplified for Bragg regime diffraction since only two principle modes were present. This allowed the single second order differential equation expressed in Equation (38) to be broken up into two first order coupled mode differential equations.

$$\frac{d}{dz}\psi^{o}(\bar{n}) = \sum_{m=1}^{N} \frac{V_m}{2L}\psi^{1}(\bar{n}+\bar{a}_m) \tag{39}$$

$$\frac{d}{dz}\psi^{1}(\bar{n}) = \sum_{m=1}^{N} \frac{V_m}{2L}\psi^{o}(\bar{n}-\bar{a}_m) \tag{40}$$

where:

u = quiescent index of refraction

ψ^{o} = zero order diffraction mode

ψ^{1} = first order diffraction mode

$\bar{n} = (n_1, n_2, \ldots\ldots n_N)$ = dimensions of the N-tuple Fourier expansion of E where n_1, n_2, etc. have integer values between $-\infty$ and $+\infty$.

$(\bar{n}-\bar{a}_m) = (n_1, n_2, .. n_{m-1}, n_m-1, n_{m+1}, n_{M-1}, n_N)$

$(\bar{n}+\bar{a}_m) = (n_1, n_2, .. n_{m-1}, n_m+1, n_{m+1}, n_{N-1}, n_N)$

Initial Conditions at z = 0 :

$$\psi^{o}(o) = 1$$

$$\psi^{1}(n) = 0$$

Hecht's results to these equations are given in terms of V_m which is "the normalized index of refraction amplitude" for the mth signal.

where:

$$V_m = Ku_mL/\cos\theta_o \tag{41}$$

u_m = refractive index perturbation due to mechanical strain caused by the mth signal.

$K = 2\pi/\lambda_o$

V_m is related to the diffraction ratio efficiency quantity by the following brief development.

$$u_m = (\frac{\partial u}{\partial s})s_m = \frac{-\eta^3 \rho s_m}{2} \tag{42}$$

where:

$$s_m = \sqrt{\frac{2I_m}{\rho V^3}} \quad = \text{mechanical strain due to mth signal}$$

(Note that V is the sound velocity)

I_m = Acoustic Intensity due to mth signal

$= P_m/LH$

Then

$$\frac{V_m}{2} = K^2 \frac{u^6 p^2 P_m L}{8H \cos^2\theta_o} \tag{43}$$

Equations (11) and (43) allow us to equate optical diffraction efficiency η_m with $\frac{V_m}{2}$. Differentiating and decoupling equations (39) and (40) enabled them to be solved with assumed power series solutions. The results for N signals were given in terms of truncated series involving V_m.

The diffraction efficiency of a single frequency component signal in the presence of N-1 other single frequency component signals was found to be the following when evaluated at z = L.

$$\frac{I_1}{I_o} = \{\psi^1(\bar{a}_1)\} \approx \{\frac{V_1}{2}\}^2\{1 - \frac{1}{3}\{\frac{V_1}{2}\}^2 - \frac{2}{3}\sum_{i=2}^{N}\{\frac{V_i}{2}\}^2\} \qquad (44)$$

$$\approx \{\frac{V_1}{2}\}^2 \quad \text{provided all } V_i < .1$$

The corresponding fractional deviation from ideal diffraction ratio of one signal due to N signals has been defined as 'compression' C.

$$C_1 = \frac{\{\frac{V_1}{2}\}^2 - I_2}{\{\frac{V_1}{2}\}^2} \approx \frac{1}{3}\{\{\frac{V_1}{2}\}^2 + 2\sum_{i=2}^{N}\{\frac{V_i}{2}\}^2\} \qquad (45)$$

'Cross modulation', m, is the compression of one signal due to a second signal only.

$$M_{1,2} = \frac{2}{3}\{\frac{V_2}{2}\}^2 \qquad (46)$$

(Self compression is not included here.)

Compression and cross modulation are important considerations in high density signal environments. Cross modulation is particularly so for optical excision applications, as an amplitude modulated interference signal of high power could do much harm to the reconstructed signal of interest.

Intermodulation is another area of concern which is described in terms of a coupled mode solution $\psi^{o}(a_1-a_2)$. Second order intermodulation products are the highest power intermods and contribute to the zero order diffraction mode. As long as $|f_2-f_1|<f_{min}$, then the second order intermod products will not be of concern. This is guaranteed if $2f_{min}>f_{max}$.

where:

f_{min} = minimum deflector passband frequency

f_{max} = maximum deflector passband frequency

This condition speaks well for deflectors having a bandwidth of slightly less than an octave. However, two-tone third-order intermods will still fall within the deflector passband and produce first order diffraction beams whose diffraction efficiency is described in terms of $\psi^{1}(2a_1-a_2)$ as follows:

$$I_{2,-1} = \psi^{1}(2a_1-a_2) \approx \frac{1}{36}\left\{\frac{V_1}{2}\right\}^{4}\left\{\frac{V_2}{2}\right\}^{2} \qquad (47)$$

Three-tone third-order intermods of the form $(f_1+f_2-f_3)$ will also create first order diffraction beams in accordance with:

$$I_{1,1,-1} = \psi^{1}(a_1+a_2-a_3) \approx \frac{1}{9}\left\{\frac{V_1}{2}\right\}^{2}\left\{\frac{V_2}{2}\right\}^{2}\left\{\frac{V_3}{2}\right\}^{2} \qquad (48)$$

As system dynamic ranges improve, third order intermodulation products will continue to become more significant.

These last remarks complete discussion on multiple frequency performance effects. Attention is now drawn to another closely related subject concerning geometric implications of light and sound interaction. Uchida [10], in his derivation of diffraction efficiency, assumed weak interaction of plane wave light incident to a rectangular sound column. The results, while very useful, do not take into account true geometric considerations of the light and sound beams. Several authors have challenged various aspects of the problem. Two particularly illuminating papers are briefly discussed here. The first paper [26] presented closed-form or analytic solutions to problems where the light and sound beams were of similar profiles.

The most common type of light-sound interaction experimentally observed is between a Gaussian profile light beam and a rectangular sound column. McMahon [26] argued that a closed-form description of this instance could not be arrived at. Instead, he proposed to bracket and indirectly analyze this case by finding solutions for two closely related cases. The two he chose were a light beam of rectangular profile intersecting a like sound column and a Gaussian to Gaussian intersection. He conducted the analysis by using an oscillating electric dipole model formulation and was able to determine the first order beam power for both situations. The following results were derived for the light beam incident at the Bragg angle so that wavevector mismatch would not have

to be considered.

For the rectangular to rectangular interaction

$$P_{rr} = A\{1 - \frac{\alpha}{3}\} \tag{49}$$

where

P_{rr} = power in first order diffraction beam for rectangular to rectangular interaction

$A = f(P_a) \frac{WL}{\cos \theta_o}^2$

$f(P_a)$ = function of input acoustic power and material constants

W = laser beamwidth

L = sound column width

$\alpha = \frac{2L\sin\theta_o}{W}$

The Gaussian-Gaussian interaction gives

$$P_{gg} = \pi^2 A/\{1 + \alpha^2\}^{\frac{1}{2}} \tag{50}$$

where:

P_{gg} = power in first order diffraction beam for Gaussian to Gaussian interaction

The author claimed for the condition of ($\frac{1}{2}<\alpha<2$) that the power diffracted by either configuration would vary from the other by no more than eight percent. Thus, by taking the mean value between them, one could only be off by about four percent from the "true" value for the intermediate Gaussian to

rectangular interaction case. However, for the deflector used in the experimental set up of this thesis, the calculated figures for the two configurations differed by a considerable margin since α was not within the specified limits.

$$W \simeq L$$

$$\theta_o = 7 \text{ milliradians}$$

$$\alpha = .014$$

$$P_{rr} = (.995)A$$

$$P_{gg} = (9.86)A$$

In spite of this variation, the results do give some insight to geometric influences on diffraction efficiency. To obtain a more general appraisal of the interaction process, Korpel's work in Ref. 27 should be consulted. He presents a technique for handling light and sound beams of arbitrary profile. The ensuing derivation assumed a spatially varying plane wave angular spectrum representation of the radiated fields and a "multiple scattering model" for the interaction process. Numerical results for particular beam configurations require power series solutions that the author left for future determination.

In conclusion, primarily qualitative benefits are available from McMahon's analysis of geometric factors. And while Korpel's theory offers exact solutions for general beam profiles, implementation may be difficult in specific cases. Much further work remains in this area.

The next and final sub-topic related to diffraction efficiency is a discussion of Bragg cell dynamic range. This

performance measure is defined as the linear operating range limited by optical background noise for minimum detectable signals and saturation for large signals. There are three types of optical scattering which are causes for background noise. Airborne dust and lens defects are scattering centers included in the first class. Their noise contribution is basically a function of the environment and component quality for a particular operating system, and so will not be considered here. By comparison, optical scattering resulting from the diffraction of the zero order beam is a function of design and is one of the two possible theoretical limits for minimum background noise. The other possible limit is scattering due to thermally generated acoustic waves in the Bragg cell medium. This type of scattering in known as Brillouin scattering. The saturation limit for large signals is determined by zero order depletion considerations in multiple frequency environments. Another maximum linear response limit could be used in signal environments composed of only one frequency component at a time, however this limit would have no practical value for typical operating conditions.

To determine a system's minimum detectable signal, both theoretical limits must be calculated and compared for the larger value. The minimum detectable signal due to zero order diffraction effects is considered first. In the worst case (maximum sidelobes), the diffraction pattern of the main beam obeys Equation (7). Sidelobe maxima are roughly determined by [20]:

$$\left.\frac{I_o(\theta)}{I_o(0)}\right|_{max} \simeq \left.\left\{\frac{\sin\pi x}{\pi x}\right\}^2\right|_{x=(N+\frac{1}{2})} \tag{51}$$

$$\simeq \left[\frac{1}{\pi N}\right]^2 \tag{52}$$

where:

$x = D\theta/\lambda_o$

N = angle of deflection due to the minimum passband frequency/angular width of a single spot and is given by $D\theta min/\lambda o$.

The point where the first order beam corresponding to the minimum passband frequency intersects the zero order diffraction pattern determines a minimum detectable signal level due to zero order interference effects. This minimum signal value relative to the axis intensity of the zero order beam was calculated as follows for the NPS a-o spectrum analyzer assuming an octave bandwidth:

Let

$I_s = I_o(\theta_{min})$ = minimum detectable signal

Then

$$\frac{I_s}{I_o(o)} = -44 \text{ dB}$$

where:

$N = D\theta_{min}/\lambda_o = 51$

$D = 7$ mm

$$\theta_{min} = \lambda_o f_{min}/(2V)$$

$$f_{min} = 2f_o/3$$

$$f_o = 80 \text{ MHz}$$

$$V = 3.63 \text{ km/sec}$$

It is important to note that the above calculated figure is independent of wavelength. The only way to lower minimum detectable signal level due to diffraction is by sidelobe reduction. For systems in which sidelobes are sufficiently attenuated, the minimum required signal would be limited by Brillouin scattering. The scattered power due to this effect is given in the following equation [28]:

$$\frac{P_T}{P_o} = \frac{8\pi FL}{3} \tag{53}$$

where:

P_T = total power scattered in all directions

P_o = incident power

F = scattering coefficient proportional to T^3

T = temperature in degrees Kelvin

L = interaction medium length

In the subsequent calculation of minimum ratio, F was not available for Lead Molybdate so a representative coefficient for a very strong scatterer was used.

$$\frac{P_s}{P_o} = \frac{2FLS}{3} = \text{normalized part of incident power delivered into one resolution cell} \tag{54}$$

$\approx$ -130 dB

where:

$F = 40\ cm^{-1}$

$L = .7$ cm

$S = \Delta\theta(1 - \cos\Delta\theta)$

$\Delta\theta = \lambda_o/L$

$\lambda_o = .6328$ um

If the two power and intensity ratios are taken to be essentially equivalent measures, then the zero order diffraction sidelobe level was clearly much stronger than the noise level due to Brillouin scattering. The upper linearity limit was determined by the maximum single frequency input allowable in a multifrequency environment which has been shown by Hecht [24] to be:

$\eta_i < .01 = -20$ dB

The resulting dynamic range (DR) calculated for the NPS Lab deflector with this condition was then:

DR = 24 dB

In general, it would appear from the above typical calculations that systems, which do not employ special sidelobe attenuation techniques, would be zero order diffraction limited in dynamic range. However, F is very temperature dependent so a unit might begin operation limited by zero order sidelobes and gradually suffer a reduction in dynamic range due to device heating.

With discussion of diffraction efficiency now completed, concentration is shifted to information capacity. This performance measure is defined as the number of beam spots resolvable in the image plane and is determined by:

$2\theta = \lambda_o/\Lambda$ = deflection angle from zero order beam

$\Delta\phi = 2(\theta_{max} - \theta_{min})$

$= \lambda_o \Delta f/V$

$N = \Delta\phi/\Delta\theta$

$= \Delta f\tau$ = number of resolvable beam spots in image plane

where:

$\tau = D/V$

D = effective aperture width

V = acoustic velocity

A large information capacity is desirable but difficult to obtain, as only two factors affect its value. Bandwidth improvement considerations have already been discussed at length under diffraction efficiency and so are not covered here. The length of time τ required for a wavefront to travel the effective length of the sound column is the principal topic of this section. To lengthen τ, a low acoustic velocity would apparently assist matters, but acoustooptic materials which have low sound velocities also tend to have high acoustic loss factors. This attenuation limits the deflector's effective aperture width and gives the sound column an exponential amplitude profile shown by:

$$A(x) = e^{-\alpha x/V} \qquad (55)$$

where:

$A(x)$ = normalized acoustic amplitude

x = distance from transducer along sound column

α = acoustic loss factor

$= \Gamma f^2 V/\{20\log_{10} e\}$ nepers/sec

Γ = material acoustic loss constant ($dB/\{cm\text{-}GHz^2\}$)

V = acoustic velocity

In order to gain a rough measure of the effective aperture's relation to acoustic loss factor, an arbitrary width was chosen where A(D) equals 2/e or approximately $1/\sqrt{2}$. Brief algebraic manipulation yields:

$$D = \{V\log_e 2\}/\alpha = 6/\{\Gamma f^2\} \tag{56}$$

The number of resolvable frequencies may now be rewritten as:

$$N = Kf_o/f^2;\ \text{let } f = f_o = K/f_o \tag{57}$$

where:

$K = 11L_o/\{V\Gamma L\}$

This result clearly shows better acoustic materials have smaller $V\Gamma$ products. It also points out for a given medium, maximum information capacity is inversely proportional to center frequency. The implication for operating systems is that once the "best" material has been selected for a normal diffraction Bragg cell then only a reciprocal relationship

exists between the system's surveillance bandwidth and information capacity. One must be sacrificed by the same percentage the other is improved. However, this last conclusion represents the ideal case, inferior performance would be observed for systems which allow thermal gradients to form during periods of high power input. In Ref. 10, Uchida presented findings on this subject which showed in one case as much as a five percent drop in information capacity for an input power increase of six percent. Proper heat sinking was reported to significantly reduce this heat dependence.

Quick response is the last general topic in the discussion of Bragg cell performance factors. This performance measure is desirable in some applications, such as Bragg cells intended to be beam modulators rather than deflectors. On the other hand, high resolution surveillance spectrum analyzers would not be noted for response agility as information capacity would directly suffer. A tradeoff must be made for optical excisors as both resolution and response speed are desirable here. For the purpose of this work, the sharpness of Bragg cell response is defined as one over τ --the rate at which single resolvable frequency inputs may be "hopped" and still attain maximum intensity diffraction ratio. It is a measure of how "instantaneous" the displayed spectrum is. The diffraction intensity of short pulses is determined by [29]:

$$I_s(t) = \int_o^D A(x,t) I_o(x) dx \qquad (58)$$

where:

$I_s(t)$ = "Short Pulse" instantaneous light intensity response

$A(x,t)$ = relative diffraction of signal in medium as a function of transited distance and time

$I_o(x)$ = incident light beam cross section in aperture

D = effective aperture width

Short pulse attenuation effects were particularly noticeable when observing the spectrum of a sinusoidally modulated FM imput signal shown in Figure 14. The input power level required an increase of nearly two orders of magnitude in contrast to the power needed for a single beam. For a qualitative overall performance comparison, a display of the same signal spectrum produced by a conventional scanning superheterodyne spectrum analyzer is presented in Figure 15.

In this section, a thorough compilation and examination of all important parameters was attempted. To summarize the findings: large information bandwidth, quick response, high diffraction efficiency and large dynamic range are functions of geometry, material constants and tradeoffs.

D. PHOTODETECTOR PERFORMANCE

The Fairchild CCD121H and Reticon CCPD-1728 photodetector arrays were the principal detectors examined in this work for spectrum analysis application. The two 1728 photosite arrays have many similar features of interest, especially in their internal working structures. Each detector photosite of both arrays integrates the current generated by the incident light.

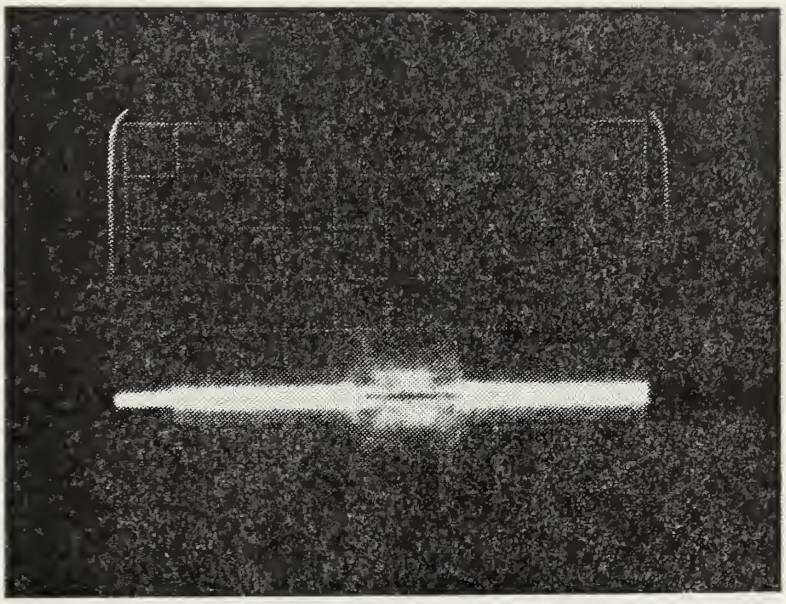

Figure 14. NPS A-O Spectrum Analyzer Display of Wideband FM Signal

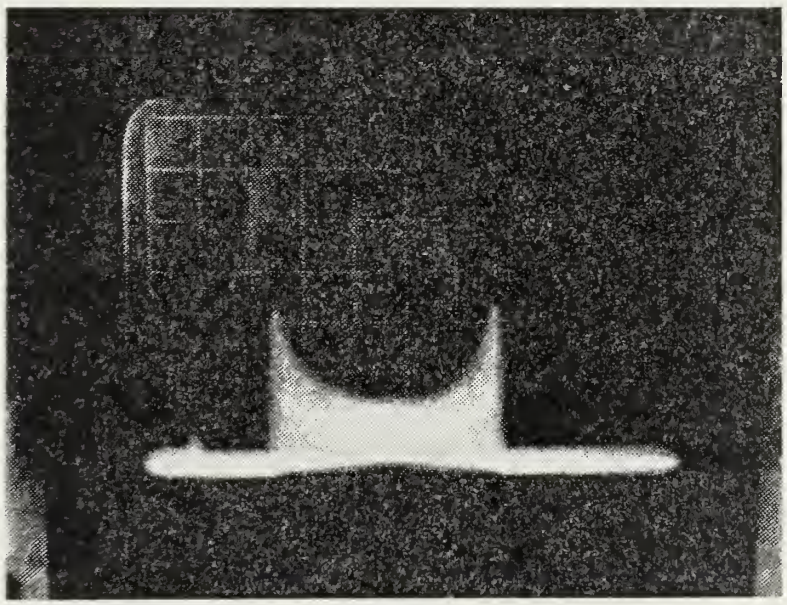

Figure 15. Conventional Spectrum Analyzer Display of Same Wideband FM Signal as in Figure 14

For this charge storage, the Reticon array photosites use photodiode junction capacitance while the Fairchild device elements rely on dielectric capacitance. Both arrays transfer the stored charge to CCD analog shift registers for further transfer to amplifying circuits and eventual display. This is accomplished by dividing the array elements into even and odd groupings. Even elements transfer to a shift register on one side of the photosite array and odd ones transfer to an opposite register. The first difference in operation occurs when the registers are transferring data off chip. The CCD chip interleaves the even and odd charge packets prior to off chip exit. The CCPD ship does not, but rather leaves this task for external circuitry. Diagrams of both chip operations are shown in Figures 16 and 17.

Examination of respective data sheets for the two devices reveals near equivalence in all specifications save two. The CCD array was a denser and faster chip. It required fourteen percent less area per photosite and used rectangular vice square shaped elements with the short dimension along the array face. This translated into a twenty percent resolution improvement over the photodiode chip. Also, the maximum output data rate of the Fairchild device was twice that of the Reticon chip. This meant better resolution of input signal temporal characteristics.

Dynamic range for both chips was defined as the individual array element's ratio of saturated output voltage to background noise equivalent voltage. The advertised dynamic range for each device was given as 27 dB. This figure was verified by

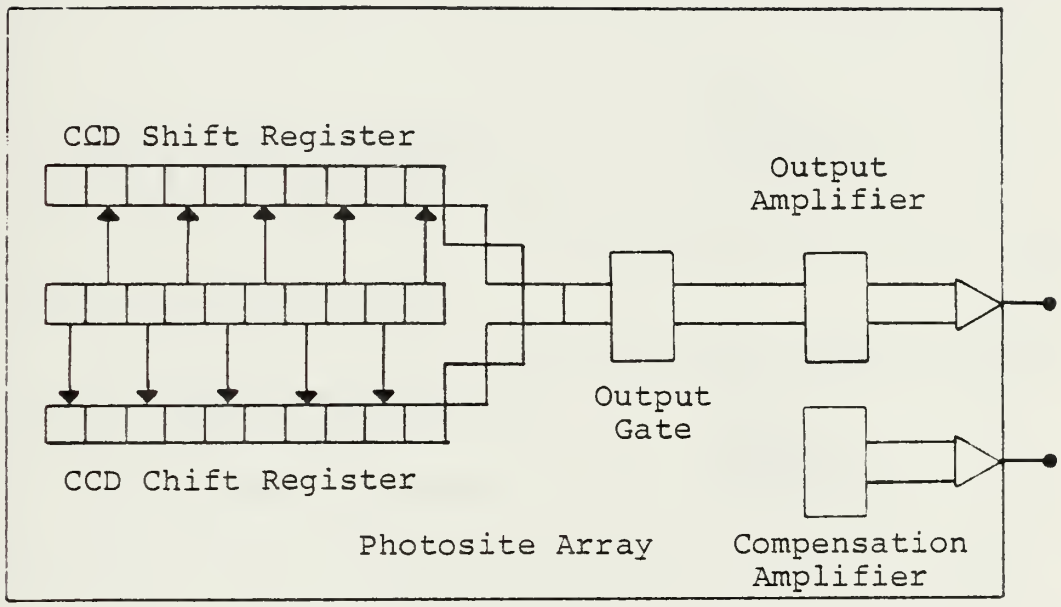

Figure 16. Fairchild Charge Coupled Device

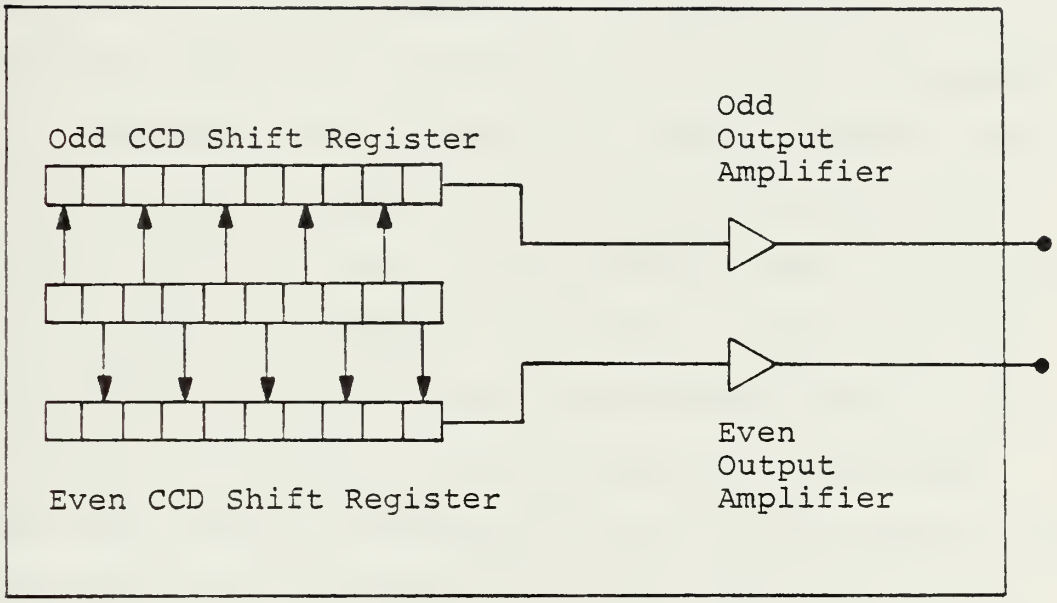

Figure 17. CCPD Photodetector Array Chip Schematic

two separate methods for the NPS spectrum analyzer CCD detector. The first method utilized the calibration marks on the rf input signal generator for this measurement. The subsequently observed dynamic range was 27.5 dB plus or minus one dB. The second technique employed neutral density filters to attenuate the saturated output signal down to the noise level and yielded a 26 dB range. However, slight beam spreading due to filter presence was noted which further attenuated the signal and accounted for the lower assessment.

Brief experience was gained with a smaller Reticon CCPD-256 chip and related support circuitry before working with the Fairchild CCD-1728 chip and development board. The photodiode array required slightly less effort to fine tune than the Fairchild model, however this may have been due to the simpler nature of the smaller device package. The larger Fairchild unit was used extensively over an eight month period and performed with 100 percent reliability throughout this time. The author believes either device technology would perform commendably in spectrum analyzer applications, but is biased in favor of the straight CCD approach in view of the above noted advantages.

Optical excisors, as noted in the introduction's list of specific goals, require a detector much different from the devices discussed above. Most excisor applications require wide information bandwidths of the kind offered by photomultiplier tubes (PMT) available on an "off the shelf" basis. For example, Varian markets typical PMTs which have bandwidths of a GigaHertz and dynamic ranges of 114 dB. These specifications

mean that a given system's performance will be most likely limited by the Bragg cell dynamic range and bandwidth. With these comments, focus is now placed on performance modeling of the optical excision process.

E. ELECTRONIC AND OPTICAL EXCISOR PERFORMANCE MODELS

Optical excision performance is measured in terms of two gauges which are: how well offending signal frequency components are removed from the output, and how much the original signal of interest is corrupted by the loss of frequency components shared with the offending signal. Both gauges are primarily functions of the electronic or optical clipper selected for use in the particular system. In this analysis, electronic clippers are assumed to completely remove interference signals chosen to be excised since nearly infinite attenuation would be available at the output ports. This same claim cannot be made for optical clippers because of diffraction limitations. The narrow obstacle of the optical clipper impedes the progress of the intended beam in much the same manner as a tree or telephone pole positioned between two people impedes dialogue. The observed diffraction effects are advantageous for conversation but not for excision.

Examination of optical clipper efficiency was approached by assuming the obstruction was much narrower than the impinging diffracted beam. In the limit, this situation may be described as a narrow obstacle in a coherent plane wave light field. Clipper effectiveness then becomes a function of the narrow obstacle width and the distance to the image

plane depicted in Figure 18. The resulting image plane intensity diffraction pattern provides a visual measure of clipper utility. This diffraction pattern was calculation in terms of Fresnel integrals where the narrow obstacle was considered to be the intersection of two overlapping infinite half planes. For further information, brief developmental guidance to derive the following image plane intensity profile is given in Ref. 17. The normalized light intensity profile, I(U) , along the u axis in the image plane (Fig. 19) is given by:

$$I(u) = \{(B - A)^2 + (2 - A - B)^2\}/4 \qquad (59)$$

where:

$$A = \int_{u_2}^{u_1} \cos\pi w^2/2 \, dw$$

$$B = \int_{u_2}^{u_1} \sin\pi w^2/2 \, dw$$

$u_2 = y_2 \{\frac{2}{\lambda r_o}\}^{\frac{1}{2}}$ = normalized integral limit

y_2= actual integral limit mapped to u_2

$\Delta y = y_1 - y_2$ = actual obstacle width

r_o= distance from obstacle to image plane

λ = light wavelength

This equation was approximated by Simpson's rule and used in a Fortran program to plot image plane intensity profiles shown in Figure 20 through 26. The figure sequence shows the effect of an obstacle which is moved steadily away from the image plane until its effect is negligible. The program

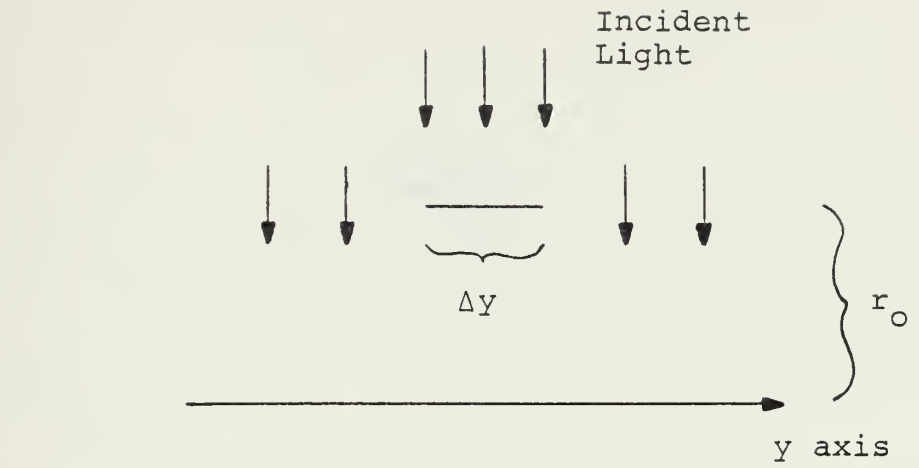

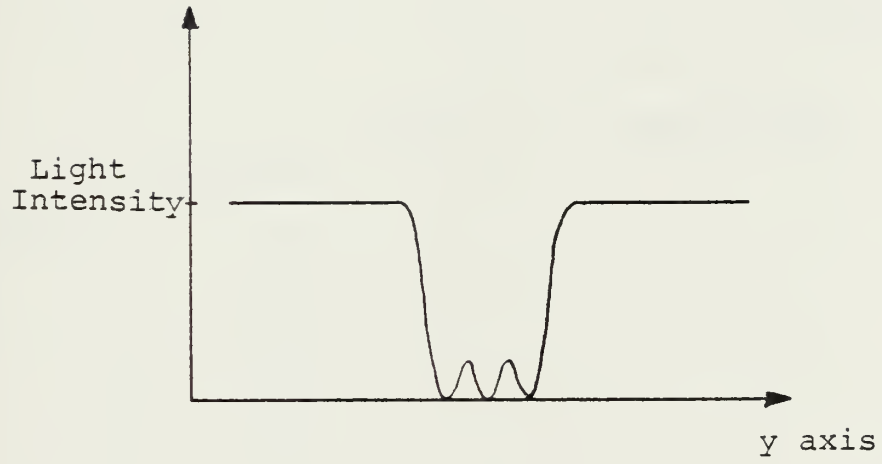

Figure 18. Narrow Obstacle in Plane Wave Light Field

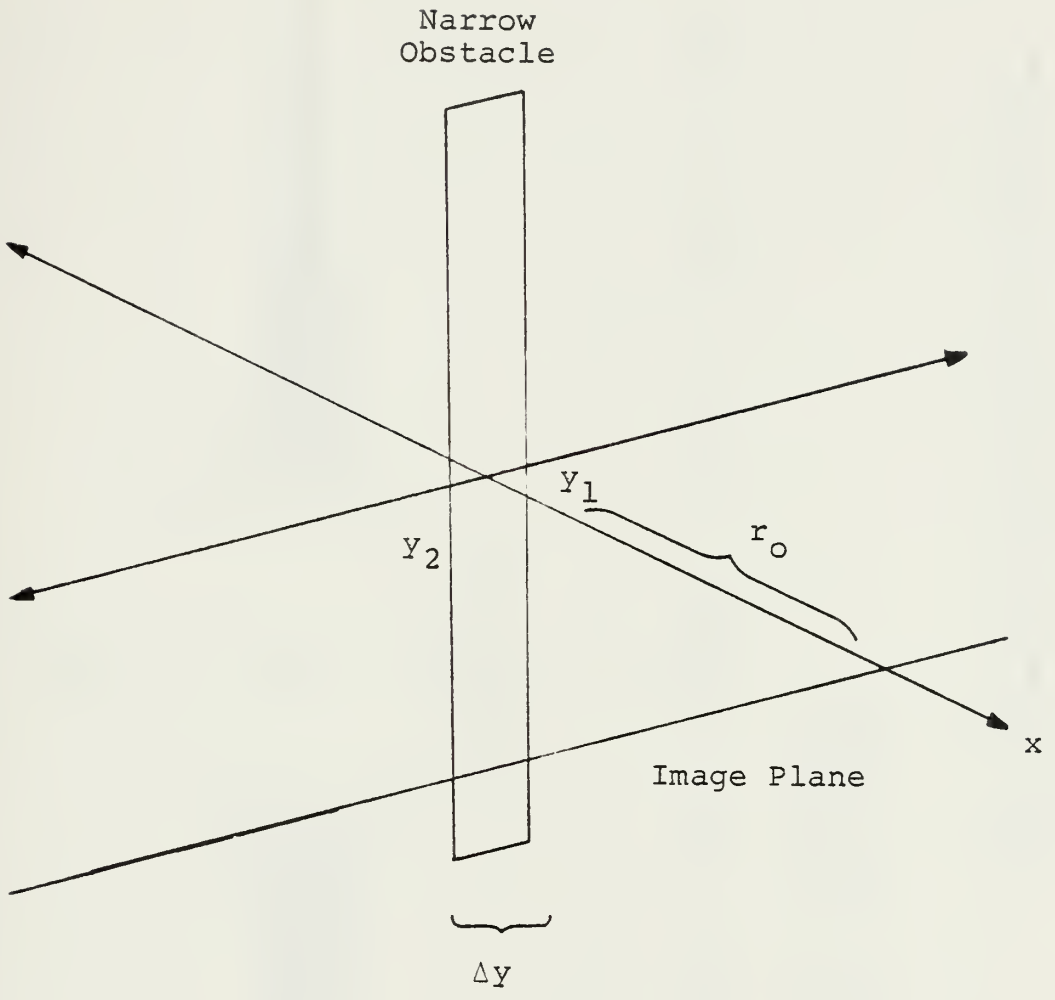

Figure 19. Narrow Obstacle Diffraction Model Schematic

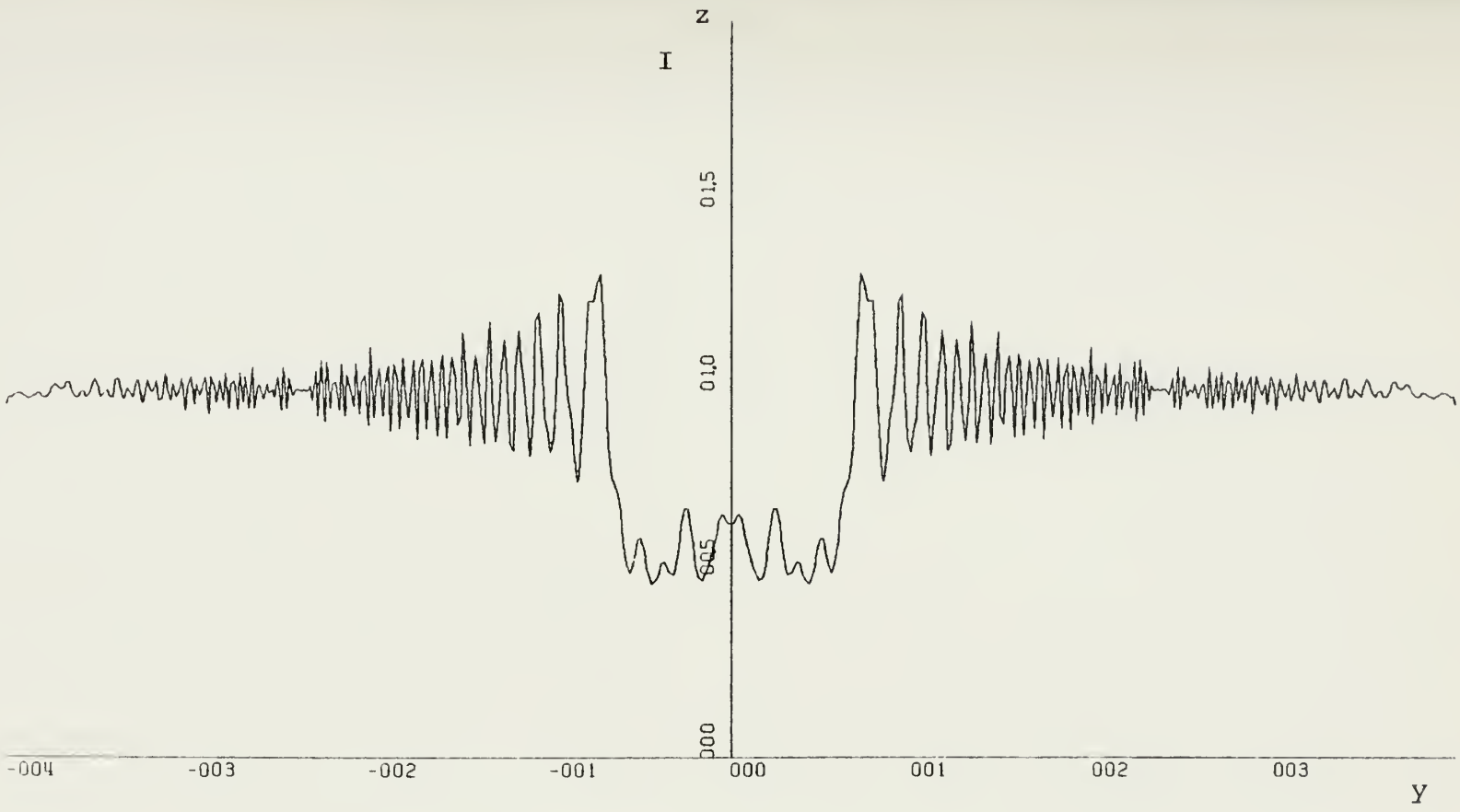

y axis - 10 um/inch

z axis - 50% Io/inch

Figure 20. Image plane intensity profile vs distance for a 16 um wide obstacle located 102.5 um in front of the image plane.

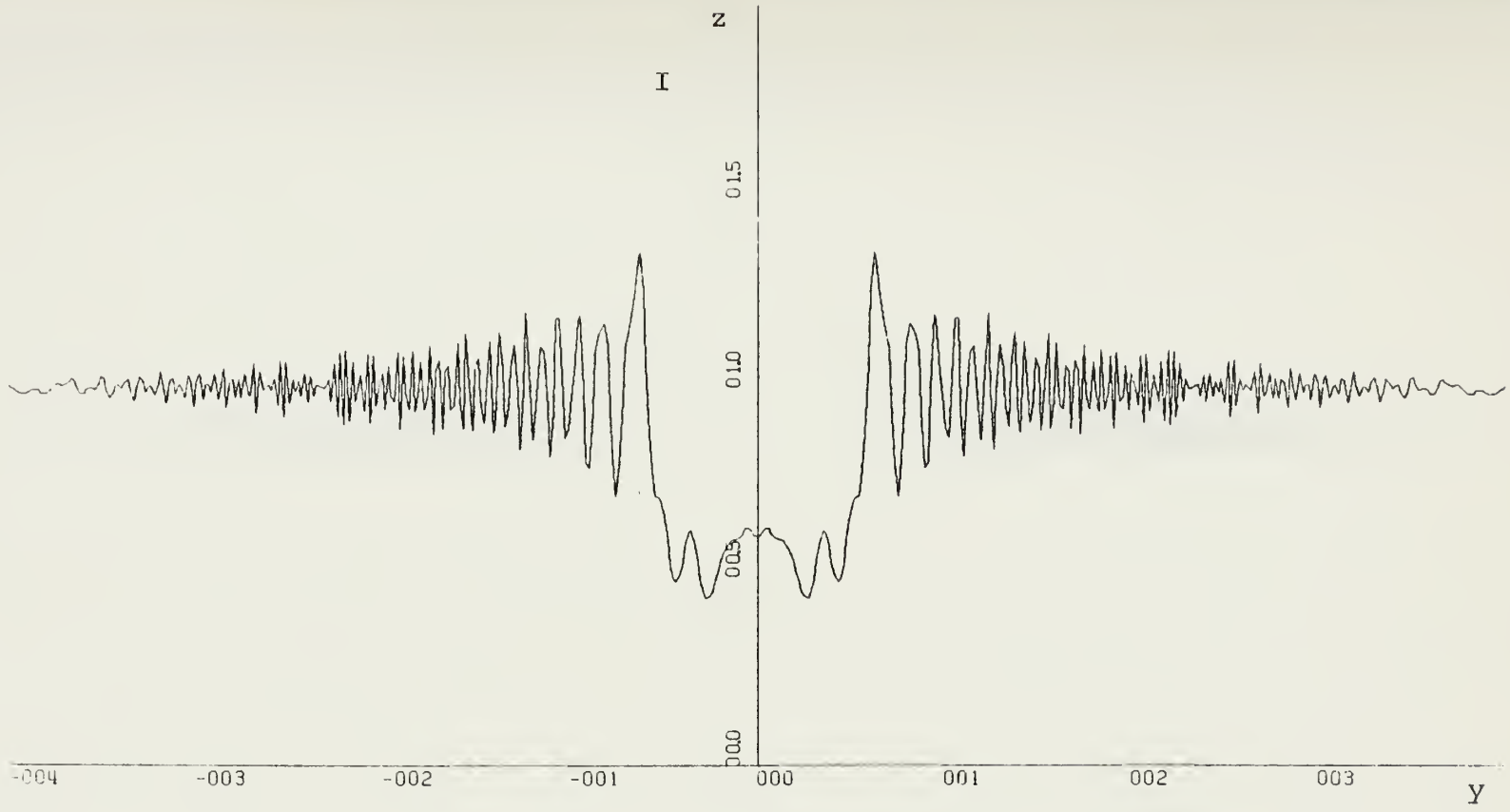

y axis - 10 um/inch

z axis - 50% Io/inch

Figure 21. Image plane intensity profile vs distance for a 16 um wide obstacle located 160 um in front of the image plane.

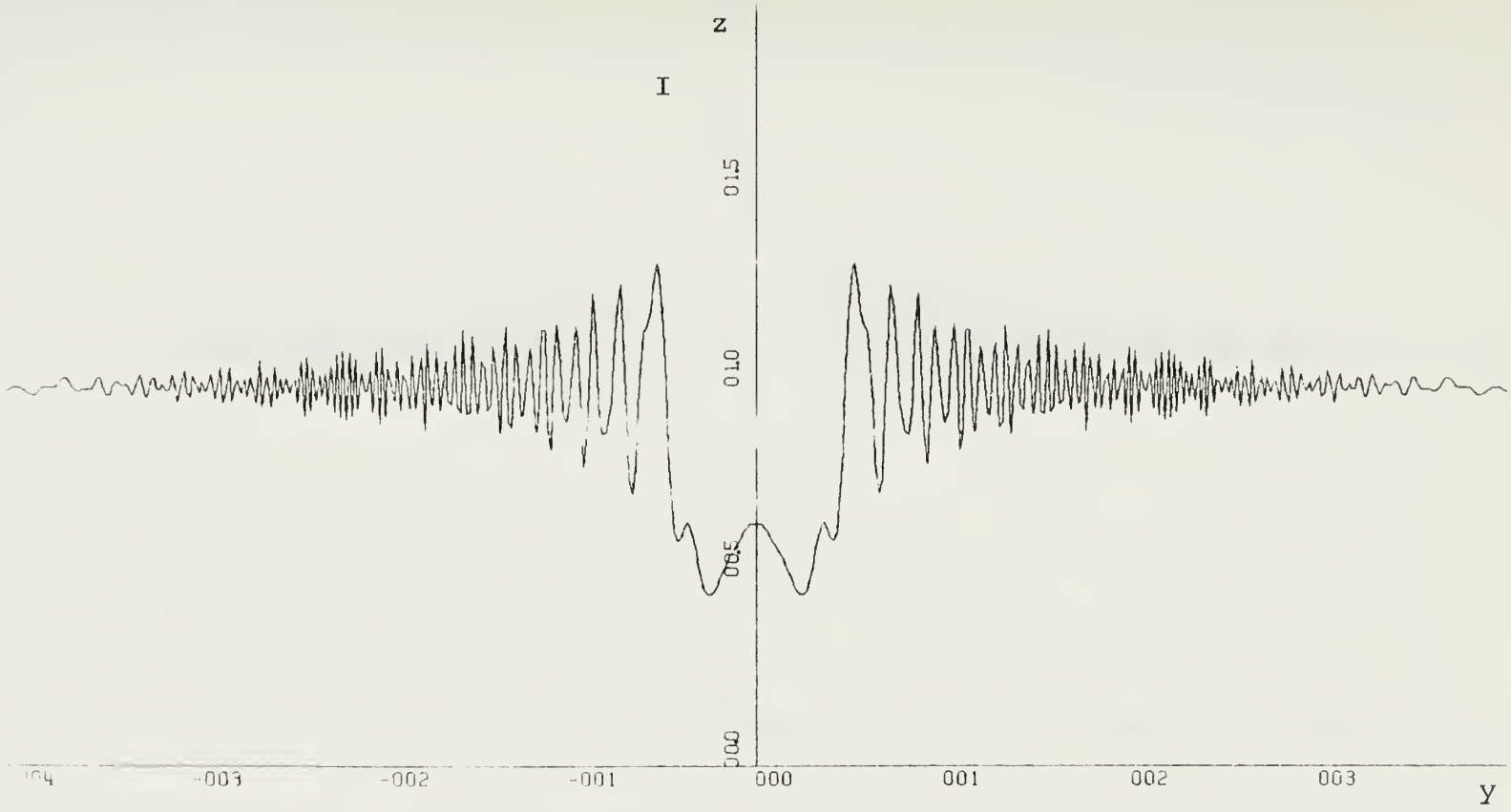

y axis - 10 um/inch

z axis - 50% Io/inch

Figure 22. Image plane intensity profile vs distance for a 16 um wide obstacle located 284 um in front of the image plane.

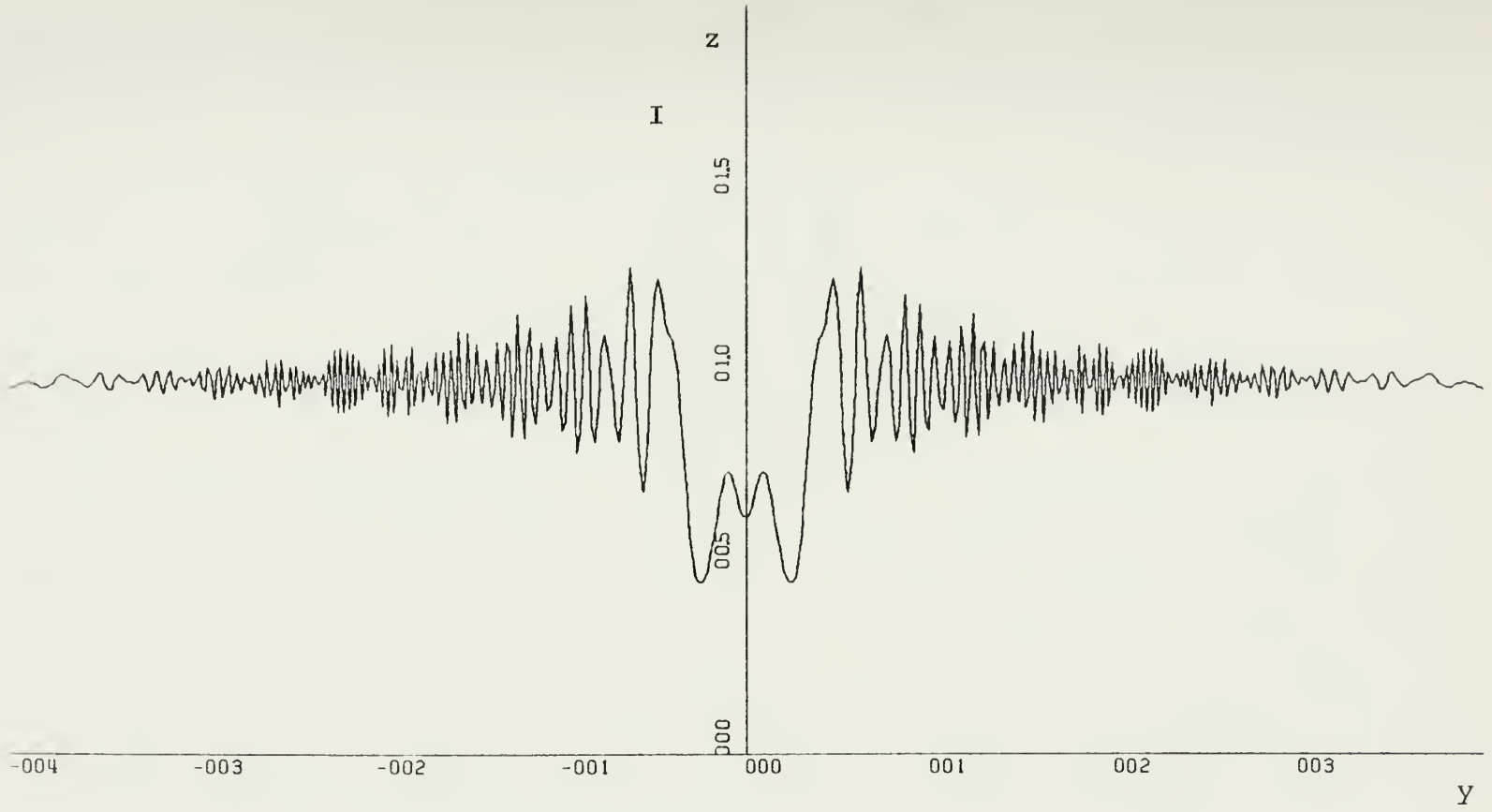

y axis - 10 um/inch

z axis - 50% Io/inch

Figure 23. Image plane intensity profile vs distance for a 16 um wide obstacle located 640 um in front of the image plane.

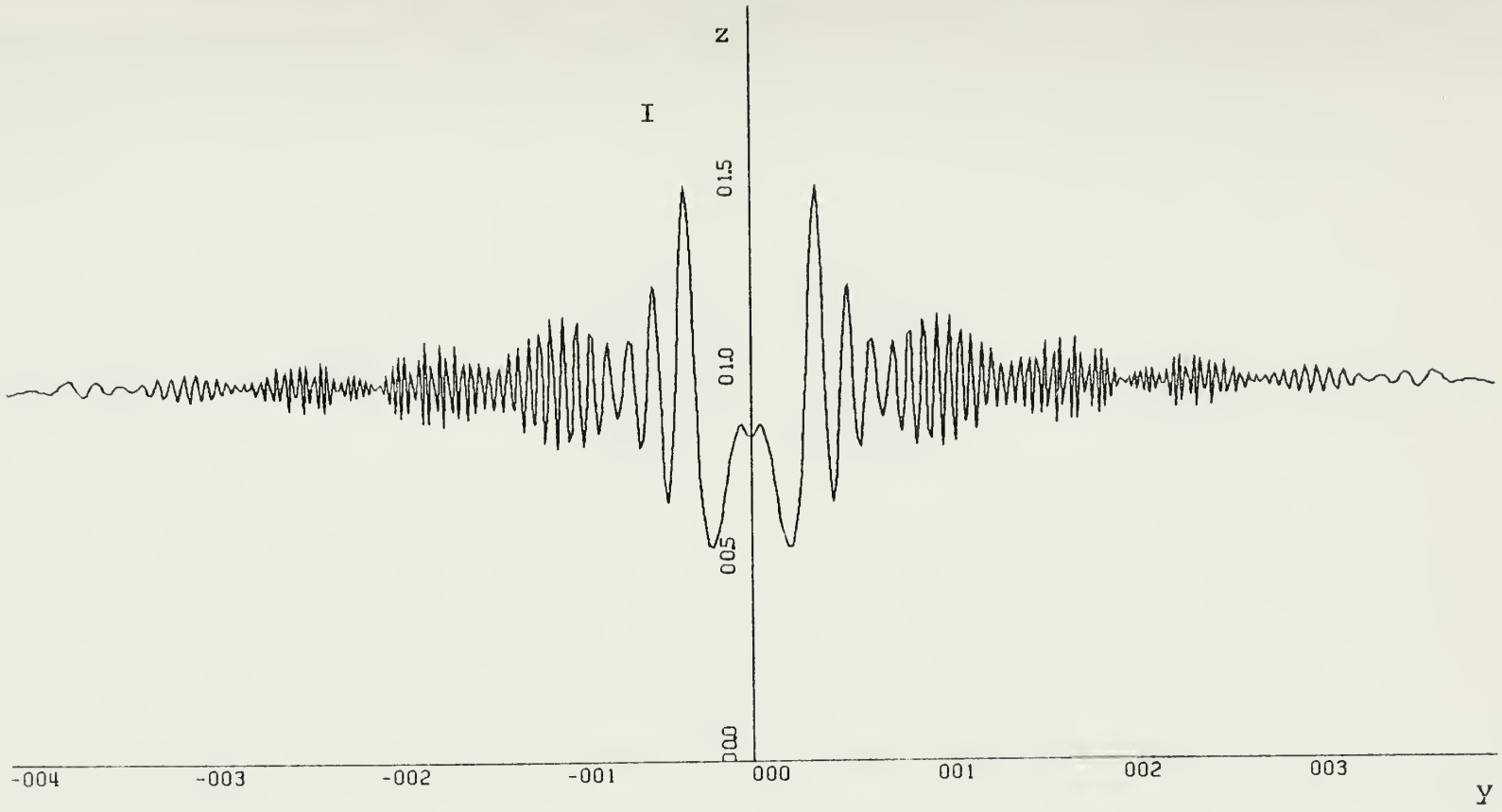

y axis - 10 um/inch

z axis - 50% Io/inch

Figure 24. Image plane intensity profile vs distance for a 16 um wide obstacle located 2.56 mm in front of the image plane.

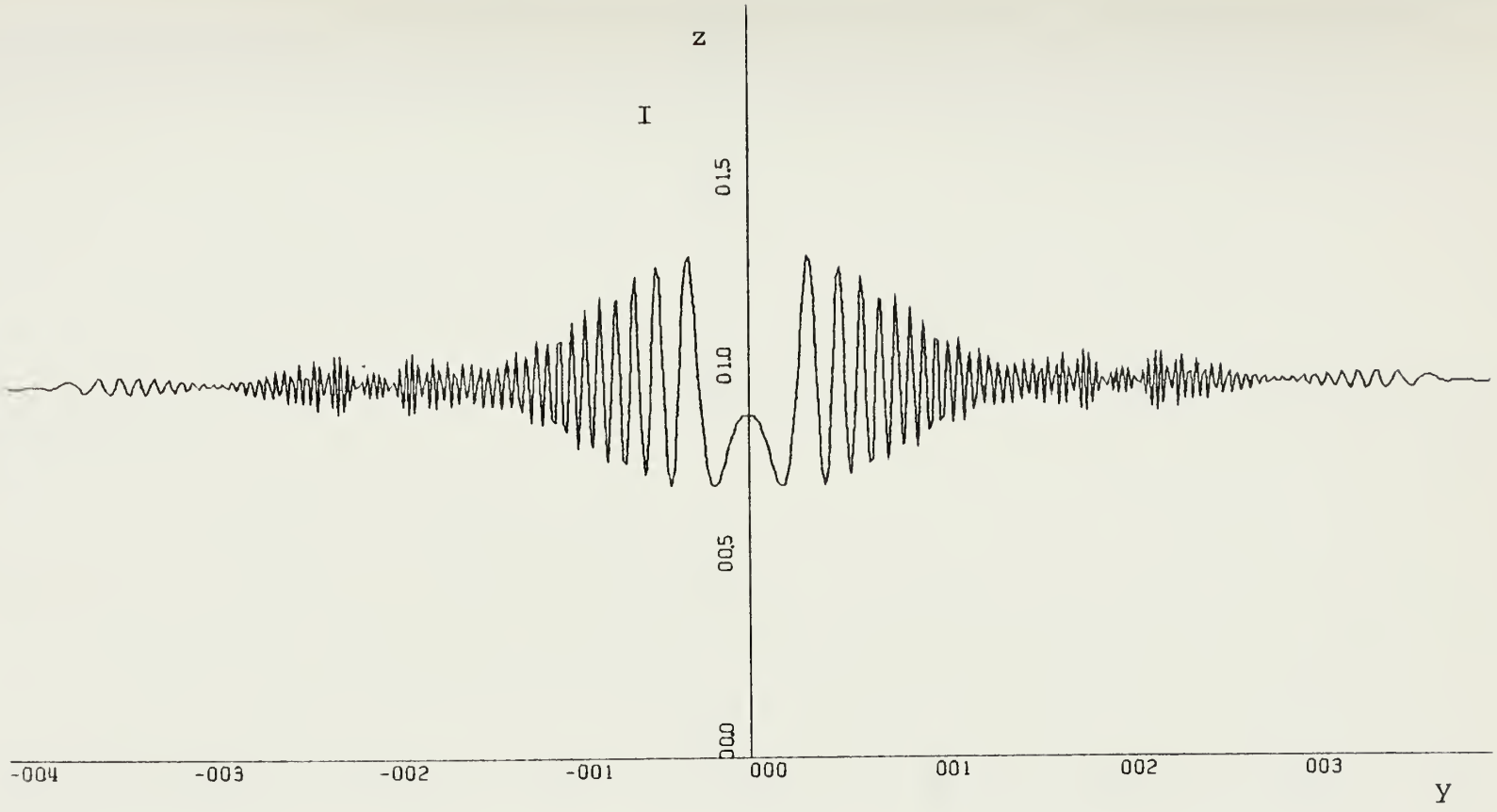

y axis - 10 um/inch

z axis - 50% Io/inch

Figure 25. Image plane intensity profile vs distance for a 16 um wide obstacle located 10.2 mm in front of the image plane.

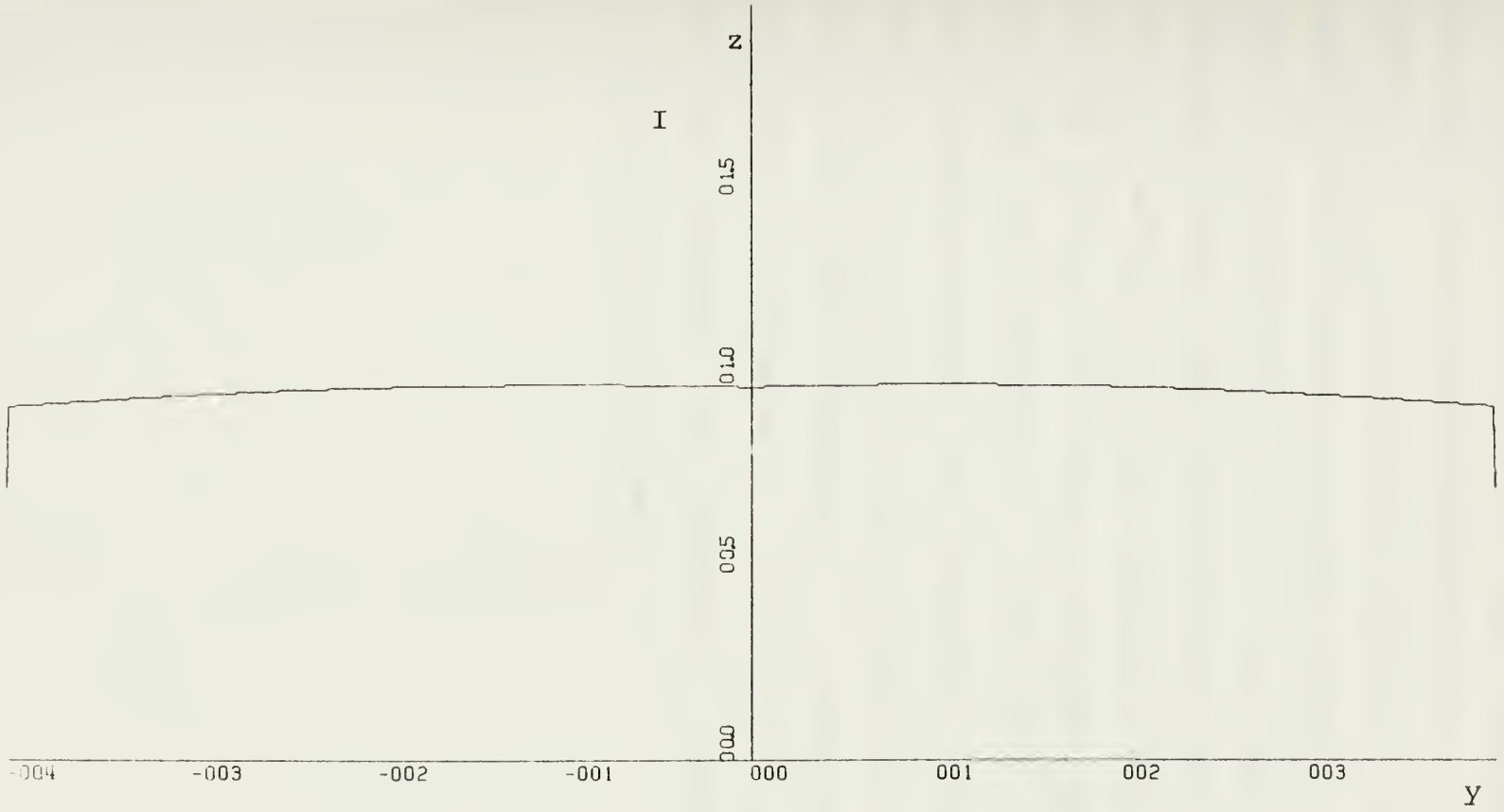

y axis - 10 um/inch

z axis - 50% Io/inch

Figure 26. Image plane intensity profile vs distance for a 16 um wide obstacle located 1.2 m in front of the image plane.

used for plotting is listed in Appendix C.

To analyze the effects of signal corruption by the excisor, the reader is directed to consult Ref. 30. In this work, Sussman and Ferrari conducted a study of Direct Sequence Spread Spectrum correlation peak attenuation due to the presence of an inband notch filter. They found that interference frequency spikes, which have bandwidths of up to three percent of the spread spectrum signal bandwidth, can be excised with only one dB drop in the output correlation peak. This worst case result was obtained for a notch filter centered on the spread spectrum signal center frequency. Much proportionately wider excision bandwidths were tolerated for slightly offset notch filter center frequencies. In conclusion, their analysis indicated the comparatively slight signal degradation due to the notch filter was much preferable to the degradation caused by the narrowband interference.

III. SUMMARY/RECOMMENDATIONS

A. RESULT SUMMARY

Laser beam propagation, Bragg cell performance, photodetector performance, and optical excision models were the main topics addressed in this work. For the laser, optimal light beam profile behavior in the image plane was found to be a function of both Gaussian beam propagation and aperture truncation effects. Observations of an assembled spectrum analyzer were made which compared closely with calculated values. And, two methods of beam sidelobe attenuation were proposed for signal resolution improvement. Bragg cell performance was measured in terms of diffraction efficiency, information capacity, and response agility. Also, device dynamic range was calculated for a multifrequency input signal environment. Additionally, beam steering and diffraction efficiency effects of light-sound beam geometric factors were studied. Photodetector array performance of charge-coupled and photodiode technologies was compared for spectrum analyzer application. Optical excisor models were discussed in terms of interference removal effectiveness and subsequent corruption of residual information bearing signals. A Fresnel approximation model of optical clipping was developed and programmed for computer plot generation. And finally, signal degradation was discussed for DSSS signal correlation peak attenuation due to excision.

B. RECOMMENDATIONS

The following remarks are specific recommendations for optimal performance of spectrum analysis, and optical excision of narrowband interference. To reduce zero order sidelobe interference, and thereby increase dynamic range, use of Bragg cell apertures which do not abruptly change in optical transmittance at the window edges is recommended. Choice of a deflector interaction medium having high refractive index, large elastooptic coefficient, small mass density, and small acoustic velocity-material acoustic loss constant produce is also desirable. Either photodetector technology was found acceptable with a slight advantage held by the charge-coupled device array. Unfortunately, no guidance can be given with regard to the choice of a "best" clipper for optical excision as developments in this area are still progressing quickly.

C. AREAS FOR FURTHER ANALYSIS

Further effort related to this thesis is required in Gaussian beam truncation analysis and electronic/optical clipping model development. A Discrete Fourier Transform (DFT) computer model of aperture windowing of Gaussian beams is one possible way of promise to study truncation effects as analytic solutions are exceptionally difficult to arrive at. Determination of window functions which "best" attenuate sidelobes and maximize information capacity would be highly desirable. Much further work also remains in optical excision modeling. Another DFT computer simulation could be used to render a Fraunhofer apploximation model of obstacle-light beam

interaction in order to further clarify optical clipper effectiveness. This approach could easily handle the case where the obstacle width would be equal to the incident light beam width. Lastly, a similar model could be used to determine nearly exact degradation effects of the excision process. These results could then determine optimal utilization of the excision process.

D. CONCLUSION

The performance analysis guidelines developed in the body of this thesis provide a realistic view of acoustooptic potential for spectrum analysis and interference excision applications. Also, several acoustooptic spectrum analyzers have been made with commercially available components and readily provide wideband, high resolution coverage not easily obtained in conventional systems. Lastly, work in optical excision techniques has progressed substantially and ongoing efforts continue to show performance improvement. In view of these facts, further research effort in this area is very likely to provide many more valuable benefits for applications involving wideband, high density signal environments.

APPENDIX A

BEAM PHASE FRONT RADIUS AND SPOT SIZE PLOT PROGRAM

This Fortran program plots Gaussian beam phase front radius and spot size as a function of distance from beam waist. Selectable parameters are:

LMBDA = laser wavelength

NPTS = number of plot points desired

WZERO = waist beam spot size

DCRM = distance increment

Prospective users at the Naval Postgraduate School should refer to the W. R. Church Computer Center's Versatec plotter routine user manual for required job control cards and plot dimensions.

```
C       BEAM RADIUS AND WAIST AS A FUNCTION OF DISTANCE
        DIMENSION R(500), X(500), W(500)
        INTEGER*4 ITB(12)/12*0/
        REAL*4   RTB(28)/28*0.0/
        RPTS = 500
        REAL LMBDA
        LMBDA  = .6328 E-06
        WZERO = .44 E-03
        LMT = NPTS + 1
        DCRM = 0.03
        PI = 3.141592654
        I = 1
        Z(1) = 1.0 E-03
  100   R(I) = Z(I) + (PI * WZERO**2/LMBDA)**2/Z(I)
        A = SQTR(1.0 + (LMBDA * Z(I)/(PI*WZERO**2))**2)
        W(I) = WZERO * 2
        I = I + I
        IF (I .EQ. LMT) GO TO 999
        Z(I) = Z(I - 1) + DCRM
        ITB(3) = 8
        ITB(4) = 4
        RTB(1) = .5
        RTB(2) = .5 E-03
        GO TO 100
  999   CALL DRAWP (NPTS,Z,W,ITB,RTB)
        RTB(2) = 5.0
        CALL DRAWP (NPTS,Z,R,ITB,RTB)
        STOP
        END
```

APPENDIX B

GAUSSIAN PROPAGATION PROGRAM

This TI-58, TI-59 hand-calculator program calculates Gaussian beam phase front radius and spot size for propagation through any number of thin lenses spaced at arbitrary distances. Selectable parameters are stored in the following registers:

*R00 = laser wavelength
R01 = beam spot size
R03 = lens focal length
R04 = distance increment

Intermediate results are stored in:

R06 = real part of complex q
R07 = imaginary part of complex q

* Common units are used throughout the program

OPERATING SEQUENCE

The wavelength of the laser is the first necessary entry. This value is entered into program memory by loading it into the display register and pressing label A. The initial beam spot size and phase front radius are entered by first keying spot size into the display and pressing B. Immediately after this, the phase front radius is loaded in the display and entered by pressing the R/S key. If the user desired to start at the waist then an infinite phase front radius can be

entered by loading any number greater than or equal to 1000, as all such values for phase front radius are treated as infinite.

The above portion of the sequence determines the initial conditions for beam propagation. From this starting point, any amount of propagation distance may be entered by loading the additional path length desired in the display and pressing D. The newly calculated beam spot size is stored in the display register and the corresponding phase front radius is stored in the t-register. Propagation through thin lenses is handled in a similar manner by entering the focal length in the display and pressing C. Spot size and phase front radius are read out in the same manner as for additional propagation distance.

The above comments complete the operating sequence description. This is now followed by a listing of the program steps by their functional sections.

SEQUENCE FOR ENTERING LASER WAVELENGTH:

*Lbl A STO 00 R/S

SEQUENCE FOR ENTERING INITIAL BEAM SPOT SIZE AND PHASE FRONT RADIUS:

"Lbl B STO 01 R/S STO 02 1000 x<>t RCL 02 *x≥t INV (RCL 02 1/x ÷ RCL 02 x^2 1/x + (RCL 00 ÷ *π ÷ RCL 01 x^2)) x^2)) STO 05

(RCL 00 ÷ *π ÷ RCL 01 x^2 ÷ (RCL 02 1/x x^2 + (RCL 00 ÷ *π ÷ RCL 01 x^2) x^2)) STO 06

CLR X<>t CLR R/S

*Lbl INV CLR STO 05 (RCL 01 x^2 x *π ÷ RCL 00)

STO 06 CLR X<>t CLR R/S

SEQUENCE FOR PROPAGATION THROUGH SPATIAL DISTANCE:

*Lbl D + RCL 05 = STO 05 E

SEQUENCE FOR CALCULATING BEAM SPOT SIZE AND PHASE FRONT RADIUS FROM COMPLEX "q":

*Lbl E ((RCL 05 x^2 + RCL 06 x^2) ÷ RCL 05) STO 02

x<>t (RCL 00 ÷ *π ÷ RCL 06 x (RCL 05 x^2 + RCL 06 x^2

)) $\sqrt{x}$ STO 01 R/S

SEQUENCE FOR TRANSMISSION THROUGH THIN LENS:

*Lbl C STO 03 (RCL 03 x^2 x RCL 06 ÷ ((RCL 03 -

RCL 05) x^2 + RCL 06 x^2)) x<>t ((RCL 03 x RCL 05

x (RCL 03 x RCL 05 x (RCL 03 - RCL 05) - RCL 03

x RCL 06 x^2) ÷ ((RCL 03 - RCL 05) x^2 + RCL 06 x^2))

STO 05 x<>t STO 06 E

APPENDIX C

BANDSHAPE PROGRAM

This Fortran program plots Bragg cell passband shapes for arbitrary integer ratios of interaction length (L) to characteristic interaction length (L_o). Selectable parameters are:

NPTS = number of plot points desired

*DLTAX = normalized frequency increment

*X(1) = normalized start frequency for plot

The number of plot lines is controlled by the limit of the second DO loop. Prospective users at the Naval Postgraduate School should refer to the W. R. Chruch Computer Center's Versatec plotter routine user manual for required job control cards and plot dimensions.

* normalized to 1

```
C  BAND SHAPE -- SINX SQR OVER X SQR
      DIMENSION X(0201), F(0201)
      INTEGER*4 ITB(12)/12*0/
      REAL*4   RTB(28)/28*0.0/
      EQUIVALENCE (TITLE,RTB(5))
      REAL*8 TITLE(12)/'BAND SHAPE'/

      NPTX = 201
      DLTAX = .01
      PI = 3.141592654
      X(1) = .1
      QPRME = 2.0 * PI
      Q = 0.0
      DO 10 I = 2, 201
      X(I) =X(I -1) + DLTAX
   10 CONTINUE
      DO  200 J = 1, 6
      Q = QPRME + Q
      DO 100 I = 1, 201
      B = (Q * (X(I) - X(I)**2) x 4.0)
      C = SIN( B )
      F(I) = ( C/B )**2
  100 CONTINUE
      IF (J .EQ. 1) ITB(1) = 1
      IF (J .EQ. 2) ITB(1) = 2
      IF (J .EQ. 6) ITB(1) = 3
      ITB(3) = 8
      ITB(4) = 4
      ITB(8) = 2
      ITB(10) = 2
      RTB(1) = .4
      RTB(2) = .4
      CALL DRAWP (NPTS,X,F,ITB,RTB)
  200 CONTINUE
      STOP
      END
```

APPENDIX D

NARROW OBSTACLE DIFFRACTION PROGRAM

This Fortran program plots diffraction patterns caused by a narrow obstacle in a plane-wave light field using a Simpson's rule approximation algorithm. Selectable parameters are:

LMBDA = laser wavelength

YMIN = left plotting boundary limit

DLTAY = obstacle width

RZERO = distance from obstacle to image plane

TNPP = total number of plotting points

TNIP = total number of integration points

Prospective users at the Naval Postgraduate School should refer to the W. R. Church Computer Center's Versatec plotter routine user manual for required job control cards and plot dimensions.

```
C NARROW OBSTACLE DIFFRACTION PROGRAM
      DIMENSION Y(500), X(500), X(500)
      INTEGER*4 ITB(12)/12*0/
      REAL*4   RTB(28)/28*0.0/
      EQUIVALENCE (TITLE,RTB(5))
      REAL*8 TITLE(12)/'DLTAY EQ 2 MICRONS RZERO EQ 19 MM'/
      REAL LMBDA
      LMBDA  = .6328 E-06
      YMIN = -40.0 E-06
      DLTAY  = 2.0 E-05
      RZERO = 19.0 E-03
      HPI = 1.570796327
      TNPP = 500.0
      TNIP = 8000.0
      STR = SQRT(2.0 / (LMBDA*RZERO)
      UMIN = YMIN * STR
      DLTAU = DLTAY * STR
      DII = DLTAU / TNIP
      DPP = -2.0 * UMIN / TNPP
      I = 1
      TUMIN = UMIN
      PUMIN = UMIN
  200 SUM1 = 0.0
      SUM2 = 0.0
  100 C1 = COS(HPI*(TUMIN**2))
      C2 = COS(HPI*(TUMIN+DII)**2)
      C3 = COS(HPI*(TUMIN+2.0*DII)**2)
      SUM1 = (C1 + 4.0*C2 + C3)*DII/3 + SUM1
      TUMIN = TIMIN + 2.0*DII
      IF (TUMIN .LE. (PUMIN + DLTAU  - 2.0*DII)) GO TO 100
      TUMIN = PUMIN
  300 S1 = SIN(HPI*(TUMIN**2))
      S2 = SIN(HPI*(TUMIN+DII)**2)
      S3 = SIN(HPI*(TUMIN+2.0*DII)**2)
      SUM2 = (S1 + 4.0*S2 +S3)*DII/3 + SUM2
      TUMIN = TUMIN + 2.0*DII
      IF (TUMIN .LE. (PUMIN + DLTAU  - 2.0*DII)) GO TO 300
      IF (I .EQ. 251) GO TO 999
      X(I) = (SUM2-SUM1)**2 + (2.0 - SUM1 -SUM2)**2
      Z(I) = X(I) / 4.0
      Z(501-I) = Z(I)
      Y(I) = (PUMIN + DLTAY / 2.0) / STR
      Y(501-I) = -Y(I)
      I = I + 1
      PUMIN = PUMIN + DPP
      NPTS = 500
      ITB(3) = 8
      ITB(4) = 4
      ITB(8) = 2
      ITB(10) = 2
      ITB(11) = 4
```

```
      RTB(1) = 1.0 E-05
      RTB(2) =    .5
      GO TO 200
  999 CALL DRAWP (NPTS,Y,Z,ITB,RTB)
      STOP
      END
```

LIST OF REFERENCES

1. Lindley, J. P. and Nurse, J. P.,"Spectrum Analysis Using Acoustooptic Techniques", Proceedings of the Society of Photo-Optical Instrumentation Engineers, Vol. 128, Effective Utilization of Optics in Radar Systems, Huntsville, Al, Sept., 1977, pp. 118-126.

2. Coppock, R. F., Croce, R. F., and Regier, W. L., "Bragg Cell RF Signal Processing", Microwave Journal, September, 1978, pp. 62-65.

3. "Bragg Cells Advancing Rapidly, Yet System Application Remains Unclear", Microwave Systems News, February, 1979, pp. 43-48.

4. Quate, C. F., Wilkinson, C. D., and Winslow, D. K., "Interaction of Light and Microwave Soung", Proceedings of the IEEE, October, 1965, pp. 1604-1622.

5. Korpel A., Adler, R., Desmeres, P., and Watson, W., "A Television Display Using Acoustic Deflection and Modulation of Coherent Light", Proceedings of the IEEE, October, 1966, pp. 1427-1437.

6. Adler, R., "Interaction Between Light and Sound", IEEE Spectrum, May, 1967, pp. 42-54.

7. Collins, W. C., Photodichroic Crystals As Adaptive Spatial Filters, U.S. Naval Research Laboratory Technical Paper.

8. Sprague, R. A., "Acoustooptic Snapshot PROM: A Real-Time Optical Signal Spectrum Analyzer", Applied Optics, 1 September 1978, pp. 2762-2767.

9. Casasent, D., "Spatial Light Modulators", Proceedings of the IEEE, January, 1977, pp. 143-157.

10. Ichida, N. and Niizeki, N., "Acoustooptic Deflection Materials and Techniques", Proceedings of the IEEE, August, 1973, pp. 1073-1092.

11. Boyle, W. S. and Smith, G. E., "Charge Coupled Semi Conductor Devices", Bell system Technical Journal, April 1970, pp. 587-593.

12. Buss, R. R., Tanaka, S. C., and Weckler, G. P., Principles of Low Noise Signal Extraction From Photodiode Arrays, Reticon Corporation Technical Paper.

13. Yariv, Amnon, Introduction to Optical Electronics, New York, Holt, Rinehart and Winston, 1976.

14. King, M., Bennet, W. R., Lambert, L. B., and Arm, M., "Real-Time Electrooptical Signal Processors", Applied Optics, August, 1967, pp. 1367-1375.

15. Benedik, G. and Greytak, T., "Brillouin Scattering in Liquids", Proceedings of the IEEE, October, 1965, pp. 143-157.

16. Siegman, A. E., An Introduction of Lasers and Masers, New York, Mcgraw-Hill, 1971.

17. Hecht, Eugene, and Zajac, Alfred, Optics, Reading, Mass., Addison-Wesley Publishing Company, 1976.

18. Born, Max and Wolf, Emil, Principles of Optics, New York, Pergamon Press, 1975.

19. Whitman, R., Korpel, A., and Lotsoff, S.,"Application of Acoustic Braff Diffraction to Optical Processing Techniques", Proceedings of the Symposium on Modern Optics, New York, New York, March, 1967, pp. 243-256.

20. Hecht, D. L., "Spectrum Analysis Using Acousto-Optic Devices", Optical Engineering, September/October, 1977, pp. 461-466.

21. Chang, I. C., "Acoustooptic Devices and Applications", IEEE Transactions on Sonics and Ultrasonics, January 1976, pp. 2-22.

22. Gordon, E. I., "A Review of Acoustooptical Deflection and Modulation Devices", Proceedings of the IEEE, October, 1966, pp. 1391-1401.

23. Pinnow, D. A., "Acoustooptic Light Deflection: Design Considerations for First Order Beam Steering Transducers, IEEE Transactions on Sonics and Ultrasonics, October, 1971, pp. 209-214.

24. Hecht, D. L., "Multifrequency Acoustooptic Diffraction", IEEE Transactions of Sonics and Ultrasonics, January, 1977, pp. 7-18.

25. Klein, W. R. and Cook, B. D., "Unified Approach to Ultrasonic Light Diffraction", IEEE Transactions on Sonics and Ultrasonics, July 1967, pp. 123-134.

26. McMahon, D. H., "Relative Efficiency of Optical Diffraction As A Function Of Interactive Geometry", IEEE Transactions of Sonics and Ultrasonics, April, 1969, pp. 41-44.

27. Korpel, A., "Two-dimensional Plane Wave Theory of Strong Acoustooptic Interaction in Isotropic Media", Journal of Optical Society of America, May 1979, pp. 678-683.

28. Benedek, G. and Greytak, T., "Brillouin Scattering in Liquids", Proceedings of the IEEE, October, 1965, pp. 1623-1629.

29. Randolph, J. and Morrison, J., "Spatial and Temporal Frequency Response of Acoustooptic Devices", Presented at Electro-Optics '71 East, New York Coliseum, Sept. 1971.

30. Sussman, S. M. and Ferrari, E. J., "The Effects of Notch Filters on Correlation Properties of a PN Signal", IEEE Transactions on Aerospace and Electronic Systems, May, 1974, pp. 385-390.

INITIAL DISTRIBUTION LIST

		No. Copies
1.	Defense Documentation Center Cameron Station Alexandria, Virginia 22314	2
2.	Library, Code 0142 Naval Postgraduate School Monterey, California 93940	2
3.	Department Chairman, Code 63 Department of Electrical Engineering Naval Postgraduate School Monterey, California 93940	1
4.	Professor John P. Powers, Code 62Po Department of Electrical Engineering Naval Postgraduate School Monterey, California 93940	5
5.	DARPA/STO 1400 Wilson Boulevard Attn: CDR Thomas F. Wiener Arlington, Virginia 22209	1
6.	Department of Defense Attn: Group R551 Fort George G. Mead, Maryland 20755	1
7.	Commander, Naval Electronic Systems Command Naval Electronic Systems Command Headquarters ATTN: ELEX-350A Washington, D.C. 20360	1
8.	Commander, Naval Electronic Systems Command Naval Electronic Systems Command Headquarters ATTN: ELEX-3501 Washington, D.C. 20360	1
9.	Commanding Officer Naval Research Laboratory ATTN: Code 7924 Washington, D.C. 20375	1
10.	Commanding Officer Naval Research Laboratory ATTN: Code 7914C Washington, D.C. 20375	1
11.	Professor W. H. Ku Department of Electrical Engineering 408 Phillips Hall Ihtaca, New York 14853	1

12. Mr. David W. Jackson 1
Probe Systems, Inc.
655 North Pastoria Avenue
Sunnyvale, California 94086

13. Lieutenant F. Weldon Regan 2
3963 North US 33
Benton Harbor, Michigan 49022